Implications of uncertain bioreactive parameters on a complex reaction network of atrazine biodegradation in soil

Giovanni Porta[a], Daniele la Cecilia[b], Alberto Guadagnini[a,c], Federico Maggi[b]

[a] *Dipartimento Ingegneria Civile e Ambientale Politecnico di Milano, Piazza L. Da Vinci, 32, I-20133 Milano, Italy*
[b] *The University of Sydney, School of Civil Engineering, Laboratory for Advanced Environmental Engineering Research, Bld J05, Sydney 2006, NSW*
[c] *Department of Hydrology and Atmospheric Sciences, University of Arizona, Tucson, AZ 85721, USA*

Abstract

We study propagation of uncertainty related to bioreactive parameters through the biodegradation reaction network of atrazine (ATZ) and its metabolites in soils. The work is motivated by the recognition that detailed analyses of these aspects in models of complex biogeochemical systems is especially critical when the feedback amongst hydraulic, chemical and microbial processes is strong. With an emphasis on microbial processes, the ATZ reaction network is exemplary because it includes 19 biological reactions mediated by 3 microbial functional groups that compete in 6 metabolic and co-metabolic degradation pathways under aerobic and anaerobic conditions. Propagation of model parametric uncertainty yields the probability distributions of ATZ, its metabolites, and the microbial biomass. It also enables us to identify key parameters that drive the long-term system dynamics. We base our analyses on an initial screening of model parameters and a subsequent moment-based global sensitivity analysis, and we show that the probability density of target outputs are multimodal as a result of nonlinearities in the degradation rate formulations. The employed global sensitivity metrics reveal that joint effects of the uncertainty of multiple kinetic parameters significantly contribute to output uncertainties, thus suggesting the presence of a high level of coupling between processes included in the network. Specific biomass affinity to a given substrate is found to be a lumped indicator that can facilitate the analysis of microbial growth when multiple and competing microbial functional groups coexist.

Keywords: Uncertainty, global sensitivity, biogeochemistry, atrazine, microbial biomass

1. Introduction

The interplay between water flow, solute transport and microbially mediated reactions is key in driving the evolution of surface and subsurface ecosystems. A proper characterization of the coupling of these processes is critical to modeling the environmental response to anthropogenic stresses in several scenarios, including managed agroecosystems, forested land [47] and aquifers [24], or when considering natural hydrometeorologic and climatic events related to climate change [18]. The capabilities of mechanistic models to describe interconnected networks of processes using first principles have rapidly increased in recent years. Accounting for an increasing number of coupled biological, chemical and physical processes is typically associated with an increasing mathematical complexity which is reflected in the number of coupled nonlinear partial differential equations used to describe individual processes. Dealing with uncertain inputs and possibly uncertain model structure is recognized as a critical issue in this broad context [e.g., 68, 40, 47, 12, 46]. While recognizing that the mathematical structure of an interpretive

model is typically uncertain in biogeochemical modeling, the distinctive aim of this study is to assess the importance of parametric uncertainty. For example, contaminant distribution in soils is the result of a feedback between transport and sorptive processes, as well as microbial processes that transform contaminants into diverse compounds at rates that are specific to a given contaminant or microbial functional group. Even if kinetic parameters can be estimated under controlled laboratory conditions, their variability in space and time at in-situ conditions may hamper the application of such estimates to predict biodegradation in natural systems. When the order of importance of one process over another changes, model outputs can also be substantially altered, depending on the sensitivity to the diverse processes represented in the model. Since a given process in a mathematical model is associated with parameters reflecting our conceptualization of the system at the scale of interest, it is important to characterize the contribution of each model parameter to the variability of target outputs. This enables us to identify potential biases, constraints, or parametric redundancies in the model formulation. In this broad framework, propagation of uncertainty through biogeochemical reaction networks is a key building block to assess the impacts of anthropogenic actions on the environment [47].

Agroecosystems are biogeochemical systems of particular interest. They are subject to natural forcing by hydrometeorological and climatic conditions, consist of highly heterogeneous soils with a wide sorptive capacity range, involve mineral and organic phases, and host a variety of both abiotic and biotic processes [66, 51, 47]. Additionally, agroecosystems are subject to anthropogenic practices of land management such as irrigations, fertigation, tillage, harvest, and pesticide applications, thus encompassing an extraordinary level of complexity that poses major challenges in the development and application of mechanistic models [54]. The use of agrochemicals simultaneously triggers the variety of processes mentioned above, with important consequences on ecosystem functioning and human health. As an example, we focus here on atrazine (ATZ). This herbicide has been banned in the European Union, but is still used at a rate of 36,000 t/year in the USA [30]. It has been demonstrated to be an endocrine disruptor, thus being potentially harmful to humans and amphibians [29, 21]. A recent contribution [35] showed that ATZ biodegradation potential and half-life can vary depending on hydrological and biogeochemical conditions, which either extend the exposure time to degrading bacteria in the top soil or reduce the transfer time to deep soil layers. Up to 97.7% of ATZ applied onto a soil can be biodegraded to its non-toxic (not containing chlorine) metabolite hydroxyatrazine (HOATZ) within the root zone, while undegraded ATZ residues and its chlorinated metabolites are transported below the root zone. ATZ biodegradation in the root zone is driven by oxidizing and hydrolizing microbial functional groups under both aerobic and anaerobic conditions along three pathways. Experimental data have been fitted to rate formulations based on Michaelis-Menten or Monod kinetics [35] but parametric uncertainty has been neglected. Previous results [34, 35] clearly show that diverse experimental datasets can lead to considerable quantitative differences in the estimated values of biokinetic parameters. Nevertheless, this information has not yet been used to perform a detailed stochastic analysis of ATZ biodegradation. It is also noted that performing field scale analyses based on reaction parameters obtained from controlled laboratory experiments may also introduce an additional bias to the estimation of the effective reaction parameters. Experiments are typically carried out under well-mixed conditions, while transport may limit reaction progress due to, e.g. incomplete mixing [13, 48, 15] as well as sorption or physical protection into soil aggregates. As an additional element of complexity, heterogeneity of natural soils at the field scale may markedly impact

effective reaction dynamics [19].

The aim of this study is to present a comprehensive analysis of the propagation of uncertainty associated with model input parameters through the systems of equations describing atrazine biodegradation in soils. We focus our analysis on (*i*) the effects of uncertainty associated with the parameters of microbially-mediated kinetic reactions, and (*ii*) the emergence of patterns in the biogeochemical response of the system under uncertainty.

To this end, we select appropriate metrics to identify (*a*) important parameters driving the system to a steady state (i.e, parameter ranking) and (*b*) the ensuing trends of selected model outputs with respect to model parameters (i.e. trend identification [6]). A discussion on available sensitivity analysis methods is presented in recent reviews [50, 6] and references therein. Given the large number of bioreactive parameters involved in our study, we apply a two-step global sensitivity analysis. We start by performing a preliminary screening to identify input parameters that provide relatively small contributions to the selected model outputs (see [9]), so as to reduce the dimensionality of the parameter space. Preliminary screenings in the context of a global sensitivity analysis have been used in previous studies to evaluate the relative importance of parameters linked to models of environmentally relevant bioreactive scenarios, including pesticide contamination of extraction wells [40], field scale bioremediation [68], and effectiveness of bioreactors [27]. We then analyze the model input-output mapping on the basis of the selected parameter set. We do so by (*a*) sampling the reduced parameter space through a standard Quasi Monte Carlo [58] approach and (*b*) quantifying global sensitivity through moment-based indices. We employ a set of the recent metrics proposed by Dell'Oca et al. [14], quantifying the relative contribution of each uncertain model parameter to main (ensemble) moments of the model output, and the Sobol' indices [57], derived from a classical decomposition of variance. The target model outputs in our long-term analyses are: average concentrations of ATZ and its chlorine-containing metabolites, and the concentrations of microbial functional groups significantly contributing to the reaction network. We then test the reliability of the specific biomass affinity, introduced by la Cecilia and Maggi [35] as an effective lumped parameter to assist characterization of microbial dynamics and prevalent reaction pathways in the presence of diverse and competing microbial functional groups.

2. Methods

2.1. The atrazine biodegradation network

We investigate parametric uncertainty in the ATZ biodegradation network integrated with the nitrogen cycle (Figure 1 after [35]). Details on the physical, chemical, and ecological conditions at the experimental site where the process was studied, parameter estimation, and modeling assumptions can be found in la Cecilia and Maggi [35]. The simulation setup is briefly recalled in 2.3. Soil and hydraulic parameters are listed in Table 1.

The general-purpose multiphase and multicomponent bioreactive transport solver BRTSim-v2.2 (based on [38]) is used for the numerical simulation of ATZ and its byproducts through the reaction network of Figure 1. Note that we refer to CH_2O as a proxy for the range of carbon-containing compounds in soil available to bacteria for growth, for simplicity. BRTSim accounts for equilibrium reactions between chemical species, including aqueous and mineral complexation, gas dissolution, and kinetic bioreactions

	West Wyalong	
Depth[a] (m)	0-1.5	1.5-5
Soil taxonomy[a]	Calcisols	Calcisols
Soil texture[a]	Clay	Loamy sand
Sand-Silt-Clay fraction[a]	15-28-57	80-10-10
Organic C fraction[a] (g-C/kg-soil)	3.9	3.9
Mineral density[b] (kg/m^3)	2849	2849
Bulk density[a] (kg/m^3)	1370	1350
Porosity[b]	0.47	0.50
Pore size distribution parameter[b]	1.43	1.74
Air entry suction[b] (m)	2.14×10^{-4}	2.37×10^{-4}
Permeability[b] (m^2) $\times 10^{-12}$	0.16	1.58

Table 1: Soil and hydraulic parameters at West Wyalong, NSW, Australia. [a] From the Harmonized World Soil Database [22]. [b] Estimated using [62].

described through Michaelis-Menten-Monod (MMM) kinetics [4, 5, 44]. The generic MMM reaction rate is expressed in BRTSim as [38]:

$$\frac{1}{x}\frac{\mathrm{d}X}{\mathrm{d}t} = r\frac{B}{Y}\prod_{n_{MM}}\frac{X_{n_{MM}}}{X_{n_{MM}}+K_{n_{MM}}\left(1+\sum_{n_{COM}}\frac{X_{n_{COM}}}{K_{n_{COM}}}\right)}\prod_{n_I}\frac{K_{n_I}}{K_{n_I}+X_{n_I}} \tag{1}$$

where X is a given chemical species concentration [mol/L], x is its stoichiometric coefficient, r [1/s] is the reaction rate constant, subscript n_{MM} refers to the half-velocity Michelis-Menten (MM) constants $K_{n_{MM}}$ [mol/L] and compounds $X_{n_{MM}}$, subscripts n_{COM} and n_I identify the competition and inhibition terms, respectively, B [mg/L] is biomass, and Y [mg$B$/mol$X$] is biomass yield. Biomass growth associated with (1) is given by

$$\frac{\mathrm{d}B}{\mathrm{d}t} = Y\frac{\mathrm{d}X}{\mathrm{d}t} - \delta_M B + b_R \tag{2}$$

where δ_M is mortality and b_R is background recovery, which are here fixed for each microbial functional group (see [35]). The structure of Eq. (1) is specific to each reaction depending on the number of MM terms, competitions, inhibitions, and microbial functional groups, and can be retrieved from the information provided in Table A.1. A MM value $K = 0.25\ \times10^{-5}$ mol/L is used for O_2(aq) consumption by microorganisms (see [8]), while O_2(aq) inhibition on anaerobic reactions is accounted for by $K_I = 0.25\ \times10^{-6}$ mol/L, along the lines of [26, 32]. The effect of pH on microbial activity is explicitly taken into account in all biologically-mediated reactions through a MM term with $K = 10^{-8}$ mol/L for high pH, and a non-competitive inhibition term with $K_I = 10^{-6}$ for low pH [35], where both terms are computed through the concentration of H^+.

The kinetic equations (1) and (2) are jointly solved in a one-dimensional (vertical) soil column coupled to fluid flow and advective-diffusive transport of aqueous compounds in variably saturated conditions [38]. The van Genuchten [62] hydraulic conductivity-saturation relationship is considered with parameters listed in Table 1. We consider water boundary fluxes which are consistent with those analyzed in [35].

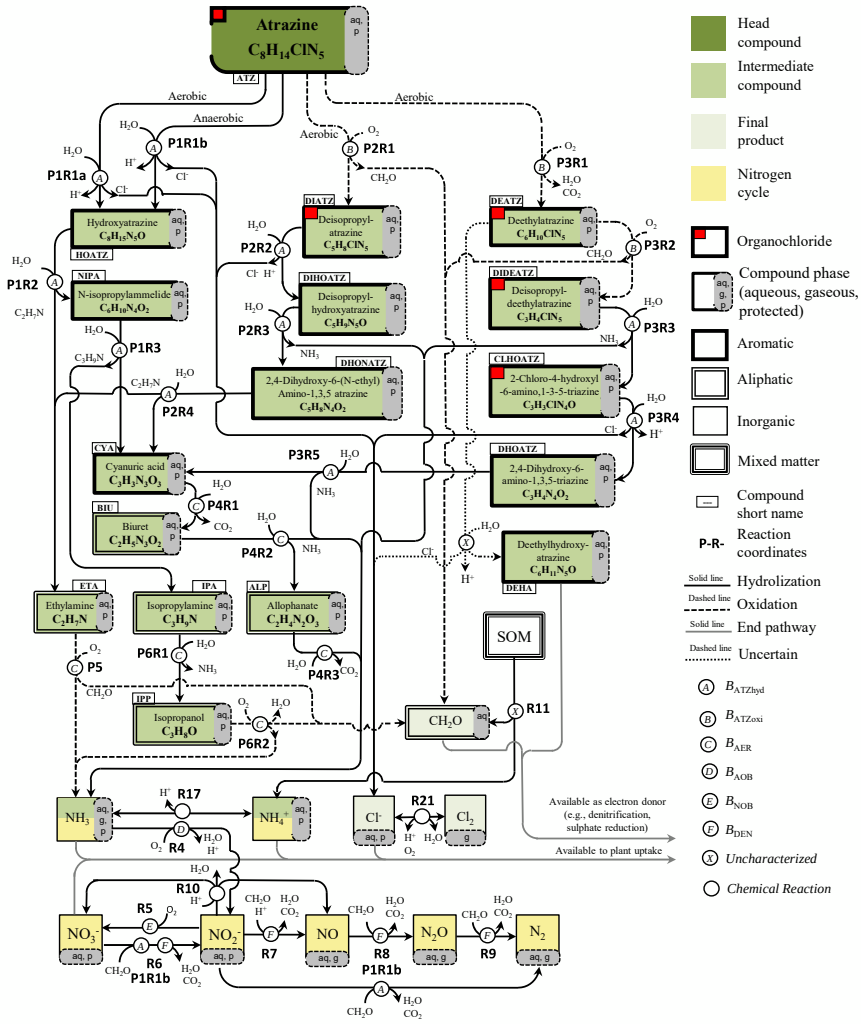

Figure 1: Atrazine biodegradation reaction network integrated with the nitrogen cycle (after [35]).

The molecular diffusion coefficient is assumed equal to 10^{-9} m^2/s for all aqueous compounds while hydrodynamic dispersion is neglected.

We consider uncertainty propagation in the biochemical reactions parameters. Stochastic simulations are implemented within the BRTSim computational environment for the reaction network of Fig. 1 upon generating a collection of random realizations of model input parameters as described in Section 2.2.

2.2. Characterization of stochastic inputs

Uncertain (stochastic) parameters selected in this study are associated with 19 kinetic reactions of ATZ and its 16 metabolites described with Eq. (1).

A total of $N_p = 74$ uncertain parameters are selected and collected in vector $\mathbf{p} = [p_1 \dots p_{N_p}]$. For convenience, the components p_k of $\mathbf{p}$ are ordered and grouped on the basis of the reactions within which they appear. Elements of groups G_1, G_2, and G_3 are parameters appearing in the reaction network along

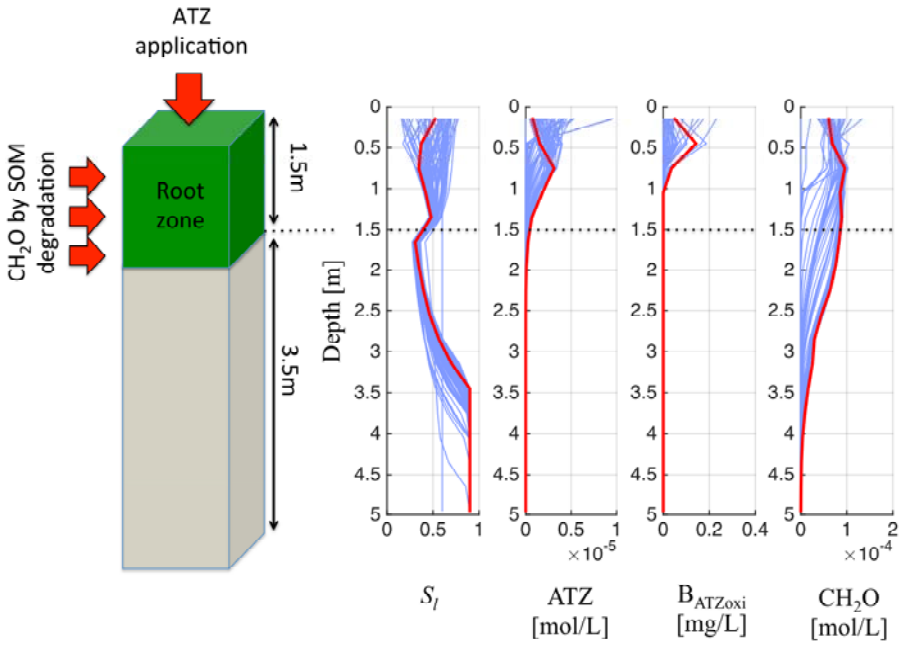

Figure 2: Sketch of the simulation setup (left) and sample profiles (right) obtained for S_l, ATZ, B_{ATZoxi}, and CH_2O for a given realization of the model parameters. The blue profiles indicate solutions associated with intermediate time steps, the red solid lines represent the solutions obtained at the final simulation time t =100y.

Group	G_1		G_2		G_3		G_4		G_5		G_6	
Parameter index, k	1 to 12		13 to 24		25 to 39		40 to 48		49 to 66		67 to 74	
Reaction mapping	P1R1	$R_{1,1}$	P2R1	$R_{2,1}$	P3R1	$R_{3,1}$	R$_1$	$R_{4,1}$	P4R1	$R_{5,1}$	P1R1b	$R_{6,1}$
	P1R1b	$R_{1,2}$	P2R2	$R_{2,2}$	P3R2	$R_{3,2}$	R$_3$	$R_{4,2}$	P4R2	$R_{5,2}$	P1R1b	$R_{6,2}$
	P1R2	$R_{1,3}$	P2R3	$R_{2,3}$	P3R3	$R_{3,3}$	R$_2$	$R_{4,3}$	P4R3	$R_{5,3}$		
	P1R3	$R_{1,4}$	P2R4	$R_{2,4}$	P3R4	$R_{3,4}$			P5	$R_{5,4}$		
					P3R5	$R_{3,5}$			P6R1	$R_{5,5}$		
									P6R2	$R_{5,6}$		

Table 2: Taxonomy of uncertain parameters and related reactions. The parameters are collected into six groups to facilitate interpretation, each parameter being identified by a corresponding index k. Each group comprises a number of reactions, labels identifying the correspondence between the biodegradation pathways defined in [35] and in Figure 1 and the nomenclature employed in this work.

pathways P1, P2 and P3, respectively (Figure 1). Group G_4 includes parameters of CH_2O metabolism, G_5 is formed by all reactions of pathways P4, P5 and P6, G_6 being defined by denitrification reactions associated with biomass growth on CH_2O. In Table 2.2 and in the rest of this work we denote the j_{th} reaction of the i_{th} group as $R_{i,j}$. Table 2.2 displays the correspondence between the nomenclature introduced here and the one employed in the reaction network depicted in Figure 1 and in [35]. We refer to Table A.1 for the detailed definition of all reactions included in the model.

Log-transformed parameter values, i.e., $\log_{10}(p_k)$, are described through a uniform probability density function within the support $\Gamma_k = [\log_{10}(\hat{p}_k) - 0.5, \log_{10}(\hat{p}_k) + 0.5]$, where $\hat{p}_k$ is the best estimate of p_k. Values of the latter are listed in Table A.1 and have been obtained in [35] through model calibration against laboratory experiments.

2.3. Simulation setup

We explore the impact of uncertainty while adopting the same simulation setup as in [35]. Figure 2 illustrates the column setup and the vertical profiles of liquid saturation S_l, ATZ, B_{ATZoxi} and CH_2O for a given parameter combinations and selected times. The simulations are run in transient conditions,

where unsteady hydrologic boundary conditions are imposed at the column top and encompass rain, irrigation and evapotranspiration. Two substrates are given as input: *i*) ATZ, which is introduced at the column top assuming an application of approximately 2 kg/ha concentrated in a single day every year, *ii*) CH_2O, which is released from the soil matrix with a constant rate (reaction R11 in Table A.1) in the root zone. The setup of the simulation ensures that a water table (attributed to locations where $S_l = 0.9$) is located at an approximately constant depth of 3.5 m. To achieve this goal, we introduce a flux term at the column bottom to balance water fluxes in the column across the simulation time window. Liquid saturation in the root zone oscillates under the effects of the unsteady boundary conditions. ATZ and biomass (illustrated here through B_{ATZoxi}) is accumulated in soil close to the top. Minimal amounts of ATZ leach to depths below 1.5 m in this particular realization of the model. The concentration of CH_2O attains a value close to 10^{-4} mol/L in the root zone and then declines with depth, due to the effect of the bottom boundary conditions (we fix a concentration of 10^{-10} mol/L in the aquifer). We emphasize that these results are only illustrative of the considered setting and are simply meant to identify general trends. The concentration values appearing in Fig. 2 are specific to the considered sample realization of the uncertain model parameters.

2.4. Target outputs

We analyze the response of the ATZ degradation network to parametric uncertainty by considering the aqueous concentration C_n of ATZ, DIATZ, DEATZ, DIDEATZ, and CHLOATZ in [mol/L] and the concentration B_s of B_{ATZhyd}, B_{ATZoxi} and B_{AER} microbial functional groups in [mg/L]. Since values of C_n and B_s typically fluctuate under the effects of prescribed hydrologic boundary conditions, we consider settings where the biogeochemical dynamics eventually attains a long-term steady-state, characterized by invariant space-time averages and only local space-time fluctuations (e.g., [35]). To this end, we run simulations spanning a 100 years time frame to reach steady state in the root zone. Average quantities over the final segment of the simulation period, i.e., $T \in [80, 100]$ years, are calculated as

$$\overline{M}_n = \int_H \frac{1}{T} \int_T C_n S_l \phi dt dz, \tag{3}$$

$$\overline{B}_s = \int_H \frac{1}{T} \int_T B_s S_l \phi dt dz, \tag{4}$$

Here, S_l is water saturation; ϕ and H respectively are soil porosity and depth; $\overline{B}_s$ [mg/m^2] and $\overline{M}_n$ [mol/m^2] respectively correspond to the total mass of microorganisms and chemicals along the soil column per unit area.

2.5. Sensitivity analysis methods

A two-step sensitivity analysis is implemented to identify important parameters among those listed in Tables 2.2-A.1. The first step relies on the approach illustrated in [45, 9, 10] and is devoted to a screening that highlights the presence of parameters with negligible influence on the results. Thus we can reduce the dimensionality of the parameter space and optimize the computational cost for global sensitivity analysis (GSA). Screening relies on the assessment of statistics of the incremental ratios $\Delta\overline{M}_n/\Delta p_k$ and $\Delta\overline{B}_s/\Delta p_k$ of the quantities defined in Eqs. (3) and (4) within the parameter space. We use the procedure described in [10] to generate a 74-dimensional quasi-random sequence and select the first $N^* = 50$ sets.

Next, we generate a second 74-dimensional quasi-random sequence, which is mixed with the first one so that parameters are changed one-at-a-time between two subsequent parameter realizations $\mathbf{p}^{i+1}$ and $\mathbf{p}^{i}$ (see [10]). We simulate ATZ degradation with BRTSim for each selected sampling point and compute the output quantities Eqs. (3) and (4). This procedure yields N^* evaluations of the incremental ratio $\Delta f(\mathbf{p})/\Delta p_k$ relative to parameter p_k. These are then used to calculate the typical screening sensitivity index [45, 9]

$$\mu_k^* = \frac{1}{N^*} \sum_{m=1}^{N^*} \left| \left[\frac{\Delta f}{\Delta p_k} \right]_m \right|, \tag{5}$$

where $f(\mathbf{p})$ is replaced either by $\overline{M}_n$ or $\overline{B}_s$.

Following screening, a moment-based global sensitivity analysis was performed for the selected group of influential model parameters. This analysis is based on $2{\times}10^4$ direct numerical simulations with parameters assigned according to a quasi Monte Carlo (QMC) sequence [58]. Equations (3) and (4) are evaluated for each of the selected parameter combinations, and are used to evaluate the sample probability density functions (pdf) of $\overline{M}_n$ and $\overline{B}_s$. The influence of each parameter on the variance of the output pdfs can be quantified through the Sobol' indices [57, 52]

$$S_k = \frac{\int_{\Gamma_k} \left(\mathrm{E}\left[f(\mathbf{p}) | p_k \right] - \mathrm{E}[f(\mathbf{p})] \right)^2 \rho(p_k) dp_k}{\mathrm{Var}[f(\mathbf{p})]}, \tag{6}$$

where Γ_k is the domain of variability of p_k, and $\rho(p_k)$ is the probability density function associated with p_k. Index S_k defines the fraction of $\mathrm{Var}[f]$ that is associated with the uncertainty of p_k and is typically defined as principal Sobol' index. The joint effect of two parameters, e.g., $[p_{k_1}, p_{k_2}]$, can be evaluated as

$$S_{k_1,k_2} = \frac{\int_{\Gamma_{k_1,k_2}} \left(\mathrm{E}\left[f(\mathbf{p}) | p_{k_1}, p_{k_2} \right] - \mathrm{E}[f(\mathbf{p})] \right)^2 \rho(p_{k_1,k_2}) dp_{k_1,k_2}}{\mathrm{Var}[f(\mathbf{p})]} - S_{k_1} - S_{k_2}. \tag{7}$$

The Sobol' decomposition allows writing the variance of each selected output as a sum of terms, each representing the contribution given by uncertain (random) inputs. According to the classical Sobol' decomposition of variance, the sum of the complete set of Sobol' indices is equal to unity [57].

A new set of sensitivity metrics (termed AMA indices by Aronne Dell'Oca, Monica Riva, and Alberto Guadagnini in Dell'Oca et al. [14]) has been recently introduced to evaluate the effects of each uncertain model parameter on given statistical moments of a random model output $f(\mathbf{p})$. We rely here on the indices $AMAE$ and $AMAV$

$$AMAE_k = \frac{\int_{\Gamma_k} \left| \mathrm{E}\left[f(\mathbf{p}) | p_k \right] - \mathrm{E}[f(\mathbf{p})] \right| \rho(p_k) dp_k}{\left| \mathrm{E}[f(\mathbf{p})] \right|}, \tag{8}$$

$$AMAV_k = \frac{\int_{\Gamma_k} \left| \mathrm{Var}[f(\mathbf{p})] - \mathrm{Var}\left[f(\mathbf{p}) | p_k \right] \right| \rho(p_k) dp_k}{\mathrm{Var}[f(\mathbf{p})]}, \tag{9}$$

where E and V respectively indicate that the index measures the importance of p_k to the mean (expected value) or variance of a model output. Positive and negative deviations of conditional mean and variance with respect to their unconditional counterparts may average out in (6). In contrast, these aspects are fully accounted for in (8)-(9) because these indices measure the modulus of the distance between conditional and unconditional statistics. Thus, relying solely on Sobol' indices might yield an incomplete

picture of a system response to the variability of model parameters, as discussed in [14]. Large values of $AMAE_k$ and $AMAV_k$ indicate that reducing (or eventually eliminating) the uncertainty associated with a given input parameter p_k leads to important effects on the sample mean and variance of model outputs. In contrast, low values of these indices indicate that efforts to characterize a given input would not lead to meaningful variations in these output statistics. In this context, GSA provides a useful framework to identify which parameters should be the target of additional investigation with the aim of increasing (a) our ability to control the output uncertainty and (b) the predictive value of model responses. These features are critical when dealing with models characterized by a large number of input parameters, such as the ATZ biodegradation network. Having at our disposal this type of information is then valuable for an effective design of laboratory- and field-scale experimental investigation and data collection.

2.6. Specific biomass affinity

We identify the specific biomass affinity associated with a bioreactive process $R_{i,j}$ as

$$\Phi_{i,j} = \frac{r^{(i,j)}}{Y^{(i,j)} K_{1_{MM}}^{(i,j)}} \tag{10}$$

where superscript (i, j) refers to the kinetic parameters of reaction $R_{i,j}$. We also introduce the dimensionless ratio, θ, between the specific biomass affinities Φ associated with two diverse biochemical reactions, e.g., $\theta_{i_2,j_2}^{i_1,j_1} = \Phi_{i_1,j_1}/\Phi_{i_2,j_2}$ (see additional details in Section 3). As noted earlier, in our analysis we have considered p_k as independent uncertain inputs. However, sensitivity indices in Eqs. (6)-(9) can also be computed also for the specific biomass affinity $\Phi_{i,j}$, instead of considering each single parameter p_k. The relationhip between the entries p_k and $\Phi_{i,j}$ is given in Eq. (10), thus implying that the domain of variability, labeled as $\Gamma^{(i,j)}$, is implicitly defined for each $\Phi_{i,j}$. Sensitivity indices computed for $\Phi_{i,j}$ are labeled as $S^{(i,j)}$, $AMAE^{(i,j)}$, $AMAV^{(i,j)}$ and are computed upon replacing p_k with $\Phi_{i,j}$ in Eqs. (6), (8) and (9), respectively. Further details on the significance of (10) are given in Appendix B.

3. Results

3.1. Screening results

Figure 3 depicts the relative importance, measured in terms of μ_k^* (Eq. (5)), of each parameter p_k to the computed values of steady-state mass of ATZ, DIATZ, DEATZ, DIDEATZ, and CLHOATZ. The high values of μ_k^* in group G4 indicate that CH_2O metabolism by B_{ATZhyd}, B_{ATZoxi} and B_{AER} has a relevant impact on the biodegradation of ATZ and its metabolites. This is consistent with CH_2O being a major carbon and energy source in microbial metabolism. Parameters in groups G_1, G_2, G_3, and G_6 display an intermediate importance. Parameters in G_5 are not relevant because they express reactions that do not directly affect biodegradation of target substrates and do not promote growth of B_{ATZhyd} and B_{ATZoxi}.

For GSA, we retain the parameters associated with bioreactive processes for which the sum of the corresponding μ_k^* values obtained for $\overline{M}_n$ exceeds 5×10^{-3} for at least one of the parameters (i.e., $r^{(i,j)}$, $Y^{(i,j)}$,$K^{(i,j)}$). Hence, we neglect 47 parameters and consider the remaining 27 parameters in the GSA.

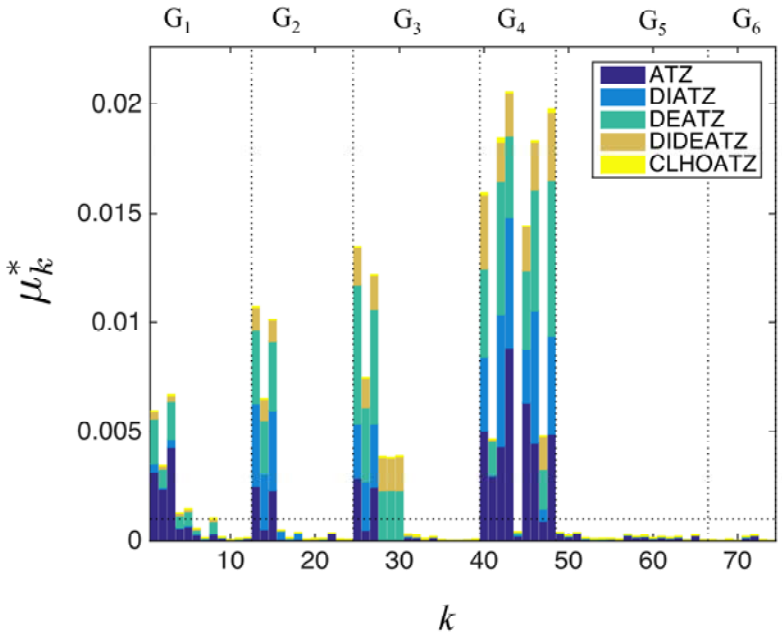

Figure 3: Screening sensitivity index μ_k^* obtained with Eq. (5) for each parameter p_k. The dashed horizontal line denotes the 5×10^{-3} threshold employed to select parameters included in the global sensitivity analysis.

3.2. Uncertainty quantification for steady-state mass of ATZ and metabolites

Figure 4 depicts the sample pdfs for $\overline{M}_n$ defined in Eq. (3), n representing ATZ, DEATZ, DIATZ, DIDEATZ, CLHOATZ. The pdf of the total mass (in moles) of chlorine-containing compounds, $\overline{M}_{\mathrm{TOT}}$, is also depicted for completeness. The pdf of $\overline{M}_{\mathrm{ATZ}}$ is unimodal and displays a single peak at a concentration of about 10^{-2} mol/m^2. Otherwise, the pdfs of $\overline{M}_{\mathrm{DIATZ}}$, $\overline{M}_{\mathrm{DEATZ}}$, $\overline{M}_{\mathrm{DIDEATZ}}$ are multimodal with a peak located around concentrations of 10^{-2} mol/m^2, and a second peak at concentrations lower than 5×10^{-6} mol/m^2. The pdf of $\overline{M}_{\mathrm{DIATZ}}$ displays a third peak around 10^{-8} mol/m^2. The pdf of $\overline{M}_{\mathrm{CLHOATZ}}$ is unimodal and spans over a narrow range of negligible mass concentration values, i.e. it is confined to values below 10^{-5} mol/m^2.

Multimodality indicates that diverse metabolites may be formed depending on the combination of model parameters. Previous results [35] indicate that negligible amounts of DIATZ, DEATZ and DIDEATZ are found when parameters are fixed to their best estimates obtained from model calibration against experimental data. The results in Figure 4 indicate that biodegradation outputs can display marked variability as a consequence of the uncertainty related to the biokinetic parameters.

The cumulative moles of chlorinated substances $\overline{M}_{\mathrm{TOT}}$ falls between 10^{-2} and 5×10^{-2} mol/m^2 for most realizations. The sample density of M_{TOT} is left-skewed thus indicating that ATZ biodegradation can produce a negligible mass of toxic metabolites for some parameter combinations. This result has important implications to bioremediation purposes because it shows that predictive modeling of bioremediation requires to properly constrain bioreactive parameters.

3.3. Global sensitivity indices related to mass of ATZ and byproducts

Figure 5 depicts the global sensitivity indices defined in Eqs. (6), (8) and (9) evaluated for $\log_{10}(\overline{M}_n)$ for ATZ, DIATZ, DEATZ and DIDEATZ. We exclude CLHOATZ from our analysis because its mass in the soil column is negligible in most cases (see Figure 4). The green bars in Figure 5 quantify sensitivity

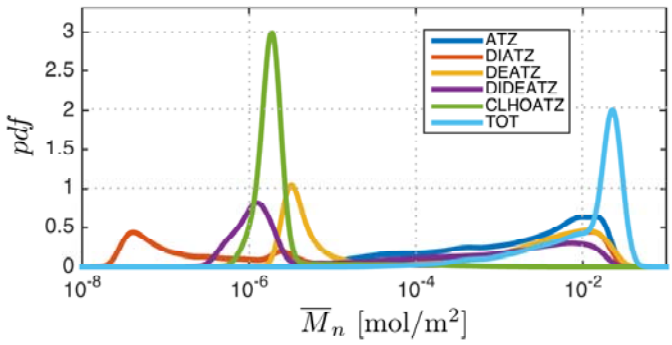

Figure 4: Sample probability density functions for $\overline{M}_n$ (n stands for ATZ, DIATZ, DEATZ, DIDEATZ, CLHOATZ and TOT).

to $\Phi_{i,j}$ (Eq. (10)) of each reaction (in terms of $AMAE^{(i,j)}$, $AMAV^{(i,j)}$, $S^{(i,j)}$), while blue bars show sensitivity with respect to the individual parameters $r^{(i,j)}$, $Y^{(i,j)}$ and $K_{1MM}^{(i,j)}$ (i.e., $AMAE_k$, $AMAV_k$, S_k). $AMAE_k$ and $AMAE^{(i,j)}$ ranging between 0.15 and 0.20 (Figure 5) imply that the output mean conditional to a single kinetic parameter or biomass affinity coefficient differs only less than 20 % from its unconditional counterpart. At the same time values of $\log_{10}(\overline{M}_n)$ display important spreading about their mean (see Figure 4). The result in Figure 5 suggests that the large variability observed in the $\log_{10}(\overline{M}_n)$ pdfs (Figure 4) cannot be explained as effects of single parameters acting separately, because interactions between parameters are important in the ATZ biodegradation network, as further discussed in Sections 3.6 and 3.7. We also note that sensitivity of the outputs to $Y^{(i,j)}$ for a given reaction $R_{i,j}$ is generally lower than that associated with $r^{(i,j)}$ and $K_{1MM}^{(i,j)}$ (i.e., in Figure 5a-d the middle blue bar tends to be smaller than the upper and lower ones for each reaction).

The highest values of the $AMAE$ indices for DIATZ, DEATZ, and DIDEATZ (Figure 5b-d) are associated with reactions $R_{4,1}$ and $R_{4,3}$, which describe CH_2O consumption. This result suggests that competition for CH_2O between B_{ATZhyd} and B_{ATZoxi} is key to determine which metabolite to expect from ATZ biodegradation. The $AMAE$ indices are consistent with the reaction network structure. For example, $\overline{M}_{\mathrm{DIATZ}}$ is influenced by parameters of $R_{2,1}$ expressing oxidative degradation of ATZ into DIATZ

(figure 5b). Degradation of ATZ into DEATZ and subsequently DIDEATZ is expressed by reactions $R_{3,1}$ and $R_{3,2}$, the parameters of which influence the average value of of $\overline{M}_{\mathrm{DEATZ}}$ and $\overline{M}_{\mathrm{DIDEATZ}}$ (figure 5c and d).

Both $AMAV_k$ and $AMAV^{(i,j)}$ are generally less selective, and tend to attain similar values for a larger number of parameters contributing to a target output. One can appraise this behavior by noting, for example, that DIDEATZ (Figure 5d) is formed by DEATZ hydrolisis by B_{ATZhyd} (see Figure 1) following ATZ oxidation by B_{ATZoxi} via reaction $R_{3,1}$. As a consequence, indices $AMAV$ indicate that the parameters of six bioreactions can contribute to a comparable extent to the variance of $\overline{M}_{\mathrm{DIDEATZ}}$. Such reactions include CH_2O consumption by three microbial functional groups ($R_{4,1}$, $R_{4,2}$, $R_{4,3}$), biodegradation of ATZ into DIATZ and DEATZ mediated by B_{ATZoxi} (reactions $R_{2,1}$ and $R_{3,1}$), and the hydrolitic reaction leading to DIDEATZ formation ($R_{3,2}$). Otherwise, Sobol' indices S indicate that $\overline{M}_{\mathrm{DIDEATZ}}$ is sensitive to parameters of $R_{4,1}$, $R_{4,3}$ and to $R_{3,1}$ to a much lesser extent.

In summary, $AMAV$ indices can capture the impact on the variability of $\overline{M}_{\mathrm{DIDEATZ}}$ due to the competition among the diverse reactive processes, a feature that is partially overlooked by quantifying the mean system behavior as embedded in the $AMAE$ indices, and neglected by principal Sobol' indices. In this context, an appraisal of the strength of the coupling between processes could also be provided by considering the Sobol' indices quantifying the combined effects of the uncertainty associated with the combination of multiple parameters characterizing the network, as we illustrate in Section 3.6.

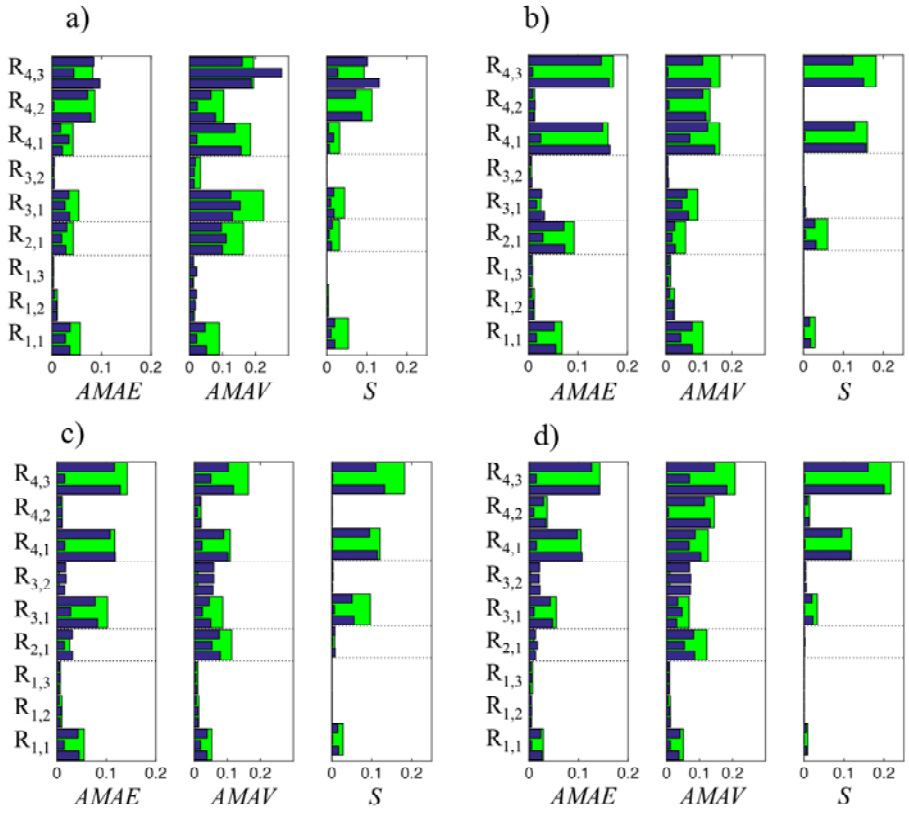

Figure 5: Principal sensitivity indices evaluated for a) $\overline{M}_{\mathrm{ATZ}}$, b) $\overline{M}_{\mathrm{DIATZ}}$, c) $\overline{M}_{\mathrm{DEATZ}}$, d) $\overline{M}_{\mathrm{DIDEATZ}}$. Green bars indicate sensitivity indices $AMAE^{(i,j)}$, $AMAV^{(i,j)}$, $S^{(i,j)}$ to the specific biomass affinity $\Phi_{i,j}$, as defined in Eq. (10). Blue bars indicate indices $AMAE_k$, $AMAV_k$ and S_k. For each $R_{i,j}$ we display three bars which express sensitivity to $r^{(i,j)}$ (bottom bar), $Y^{(i,j)}$ (middle bar) and $K_{1MM}^{(i,j)}$ (top bar). Only sensitivity to $r^{(i,j)}$ is expressed for $R_{6,1}$.

3.4. Uncertainty in biomass at steady-state

Figure 6 depicts the sample pdfs of the biomass $\overline{B}_s$ (where s stands for ATZhyd, ATZoxi, and AER) together with the pdf of the cumulative biomass $\overline{B}_{\mathrm{TOT}} = \overline{B}_{\mathrm{ATZhyd}} + \overline{B}_{\mathrm{ATZoxi}} + \overline{B}_{\mathrm{AER}}$. The remaining three functional groups are mostly unaffected by the investigated parametric uncertainty and are neglected in this analysis. The pdfs of $\overline{B}_{\mathrm{ATZhyd}}$, $\overline{B}_{\mathrm{ATZoxi}}$ and $\overline{B}_{\mathrm{AER}}$ are multimodal. The pdf of $\overline{B}_{\mathrm{ATZoxi}}$ displays three clearly distinguishable peaks, while the pdf of $\overline{B}_{\mathrm{TOT}}$ is unimodal.

The three densities $\overline{B}_s$ as well as $\overline{B}_{\mathrm{TOT}}$ display a peak at about 10^2 mg/m^2. Note that the three functional groups $\mathrm{B}_{\mathrm{ATZhyd}}$, $\mathrm{B}_{\mathrm{ATZoxi}}$ and $\mathrm{B}_{\mathrm{AER}}$ compete for CH_2O in reactions $R_{4,1}$, $R_{4,2}$, $R_{4,3}$, the parameters of which are randomly sampled across the same domain of variability (see Table A.1). This result suggests that the rightmost peak of each distribution is associated with assimilation by $\mathrm{B}_{\mathrm{ATZhyd}}$ and $\mathrm{B}_{\mathrm{ATZoxi}}$ of CH_2O rather than ATZ. The cumulative biomass $\overline{B}_{\mathrm{TOT}}$ attains values always larger than 10 mg/m^2 and ranges between 2×10 and 2×10^2 mg/m^2, because bioavailable CH_2O always supports growth of at least one functional group among $\mathrm{B}_{\mathrm{ATZhyd}}$, $\mathrm{B}_{\mathrm{ATZoxi}}$ and $\mathrm{B}_{\mathrm{AER}}$, for any parameter combination.

The pdf of $\overline{B}_{\mathrm{ATZoxi}}$ shows a marked intermediate peak at concentrations close to 1 mg/m^2. We also observe an intermediate peak in the pdf of $\overline{B}_{\mathrm{ATZhyd}}$ that might be partially overlapped with the rightmost peak. A peak corresponding to intermediate concentration values does not appear in the density of $\overline{B}_{\mathrm{AER}}$. Therefore, one can conclude that the occurrence of a third peak for intermediate values of $\overline{B}_{\mathrm{ATZoxi}}$ and $\overline{B}_{\mathrm{ATZhyd}}$ might be associated with sample realizations in which $\mathrm{B}_{\mathrm{ATZoxi}}$ and $\mathrm{B}_{\mathrm{ATZhyd}}$ grow on ATZ and its metabolites.

The pdfs of $\overline{B}_s$ display a leftmost peak in the low concentration values. This is related to parameter sets for which a given functional group is outscored by the others in the competition for all available substrates. Note that each functional group is prevented to reach a null biomass concentration by imposing a fixed background recovery parameter. $\mathrm{B}_{\mathrm{AER}}$ biomass has a lower bound of nearly 1 mg/m^2 but still larger by a factor of 10^3 than the minimum observed for $\mathrm{B}_{\mathrm{ATZoxi}}$ and $\mathrm{B}_{\mathrm{ATZhyd}}$. This difference reflects the assumed difference in the background recovery imposed in the biomass dynamics (Eq. (2)).

3.5. Global sensitivity indices of biomass

Figure 7 depicts the set of global sensitivity indices evaluated for $\log_{10}(\overline{B}_{\mathrm{ATZhyd}})$, $\log_{10}(\overline{B}_{\mathrm{ATZoxi}})$, $\log_{10}(\overline{B}_{\mathrm{AER}})$ and $\log_{10}(\overline{B}_{\mathrm{TOT}})$. The biomass of all microbial groups in the soil column is mainly influenced by the parameters of group G_4, which express the kinetics of CH_2O metabolism via reactions $R_{4,1}$, $R_{4,2}$, $R_{4,3}$. In particular, $R_{4,1}$ and $R_{4,3}$ influence the steady-state biomass of $\mathrm{B}_{\mathrm{ATZhyd}}$ and $\mathrm{B}_{\mathrm{ATZoxi}}$, which is consistent with the reaction network structure. This result shows that the dominant process leading to biomass growth is CH_2O assimilation and is consistent with the shape of the sample pdfs of biomass (see also Section 3.4). We find that sample mean and variance of $\overline{B}_{\mathrm{ATZhyd}}$ and $\overline{B}_{\mathrm{ATZoxi}}$ are also sensitive to parameters of $R_{1,1}$, $R_{2,1}$ and $R_{3,1}$ expressing growth on ATZ hydrolysis and oxidation (Figure 7a).

The mean and variance of $\overline{B}_{\mathrm{TOT}}$ are almost exclusively influenced by parameters in group G_4, and mostly by $Y^{(i,j)}$ relative to $R_{4,1}$, $R_{4,2}$ and $R_{4,3}$. This implies that the variability of $\overline{B}_{\mathrm{TOT}}$ depends on the ability of each functional group to maximize its growth per unit mass of consumed CH_2O. In turn, it suggests that the reaction is likely to be substrate-limited (most likely due to limitations in the mass transfer between soil organic matter and CH_2O, although transport limitations may also occur at specific times) in the considered final equilibrium stage because $r^{(i,j)}$ and $K_{1MM}^{(i,j)}$ do not influence the

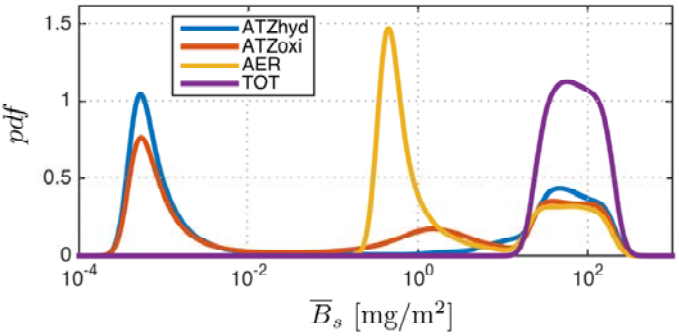

Figure 6: Sample probability density functions for $\overline{B}_s$ (s stands for ATZhyd, ATZoxi, AER, and TOT).

total biomass and therefore the total CH_2O consumed. Otherwise, in a rate-limited case, a variation in $r^{(4,1)}$, $r^{(4,2)}$, $r^{(4,3)}$ would yield changes in $\overline{B}_{\mathrm{TOT}}$.

3.6. Analysis of processes interaction

Results in Sections 3.3 and 3.5 suggest that the effects of the interactions among diverse reactions is significant for the considered outputs. Here, we provide additional insights on this aspect through the Sobol' decomposition, or analysis of variance (ANOVA). We consider the specific biomass affinities $\Phi_{i,j}$ as input stochastic variables, rather than individual kinetic parameters. This choice is motivated by the observation that the value of $\Phi_{i,j}$ is tied to a characteristic time scale of each considered bioreactive process, as recalled in Appendix B.

Since the sum of the complete set of Sobol' indices is equal to one for each target output, we distinguish the contribution given by three subsets of indices in Fig. 8 as a function of the number of reactions n_R (or biomass specific affinities $\Phi_{i,j}$) which they depend on. These subsets are (a) principal Sobol' indices, describing the effect of each $\Phi_{i,j}$ associated with a single reaction (blue bars, $n_R = 1$), (b) two reactions (green bars, $n_R = 2$) or (c) more than two reactions (red bars, $n_R > 2$). This analysis indicates the strength of coupling between processes included in the reaction network. We observe that the sum of all indices which embed variations of more than one $\Phi_{i,j}$ (green and red bars) is larger than 0.5 for all

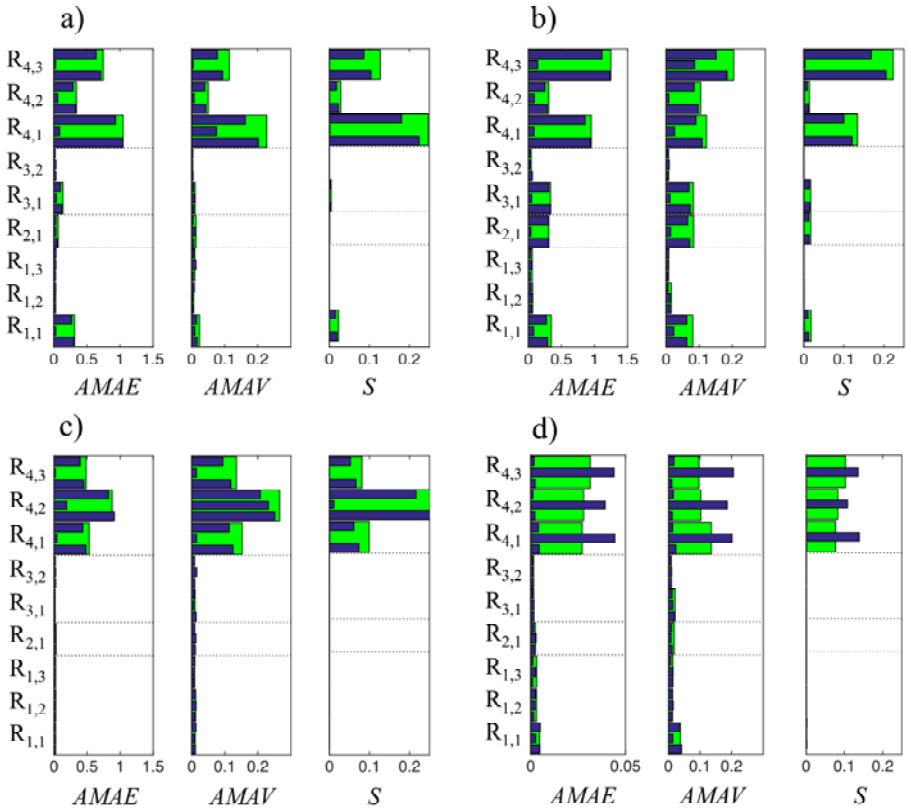

Figure 7: Principal sensitivity indices evaluated for a) $\overline{B}_{\mathrm{ATZhyd}}$, b) $\overline{B}_{\mathrm{ATZoxi}}$, c) $\overline{B}_{AER}$, d) $\overline{B_T}$. Green bars indicate sensitivity indices $AMAE^{(i,j)}$, $AMAV^{(i,j)}$, $S^{(i,j)}$ to the specific biomass affinity $\Phi_{i,j}$, as defined in Eq. (10). Blue bars indicate indices $AMAE_k$, $AMAV_k$ and S_k. For each $R_{i,j}$ we display three bars which express sensitivity to $r^{(i,j)}$ (bottom bar), $Y^{(i,j)}$ (middle bar) and $K_{1MM}^{(i,j)}$ (top bar). Only sensitivity to $r^{(i,j)}$ is expressed for $R_{6,1}$.

outputs, i.e. joint variations of two or more parameters $\Phi_{i,j}$ contributes (on average) to more than 50% of the variance of the selected outputs. We also observe that the sum of indices associated with more than two reactions ($n_R > 2$, Fig. 8) ranges between 0.4 and 0.5 for all of the outputs considered.

3.7. Impact of biomass affinity

The most important reactions in the network are those in G_4, which are associated with CH_2O consumption (see results Sections 3.3 to 3.5). We recall that equal kinetics of CH_2O consumption were assumed in [35] for the three bacterial functional groups, i.e. $\Phi_{4,1} = \Phi_{4,2} = \Phi_{4,3}$. We investigate here the effect of the variability in $\Phi_{4,1}$, $\Phi_{4,2}$, $\Phi_{4,3}$ on the selected outputs.

We analyze contour maps of the average biomass $\overline{B}_{\mathrm{ATZhyd}}$, $\overline{B}_{\mathrm{ATZoxi}}$, $\overline{B}_{\mathrm{AER}}$ conditional to the specific biomass affinities $\Phi_{4,1}$ and $\Phi_{4,3}$ (Figure 9). In the same Figure 9a-c also depicts contours associated with the average values of $\overline{M}_{\mathrm{ATZ}}$ (in white) and $\overline{M}_{\mathrm{DIATZ}}$ (in red) conditional to $\Phi_{4,1}$ and $\Phi_{4,3}$. This result allows identifying regions of the parameter space where either oxidative or hydrolytic processes can be expected to prevail in the ATZ biodegradation reaction network because of the competition between $\mathrm{B_{ATZoxi}}$ and $\mathrm{B_{ATZhyd}}$ for CH_2O. The smallest values of the conditional mean of $\overline{B}_{\mathrm{ATZhyd}}$ are associated with large values of $\Phi_{4,3}$ and small values of $\Phi_{4,1}$ (top left corner in Figure 9a). The minimum value of the conditional biomass average of $\overline{B}_{\mathrm{ATZhyd}}$ is approximately 10^{-3} mg/m^2, which corresponds to the location of the leftmost peak of the pdf of $\overline{B}_{\mathrm{ATZhyd}}$ depicted in Fig. 6. These low biomass values are likely associated with $\mathrm{B_{ATZhyd}}$ close to the background recovery concentration. We find largest values of

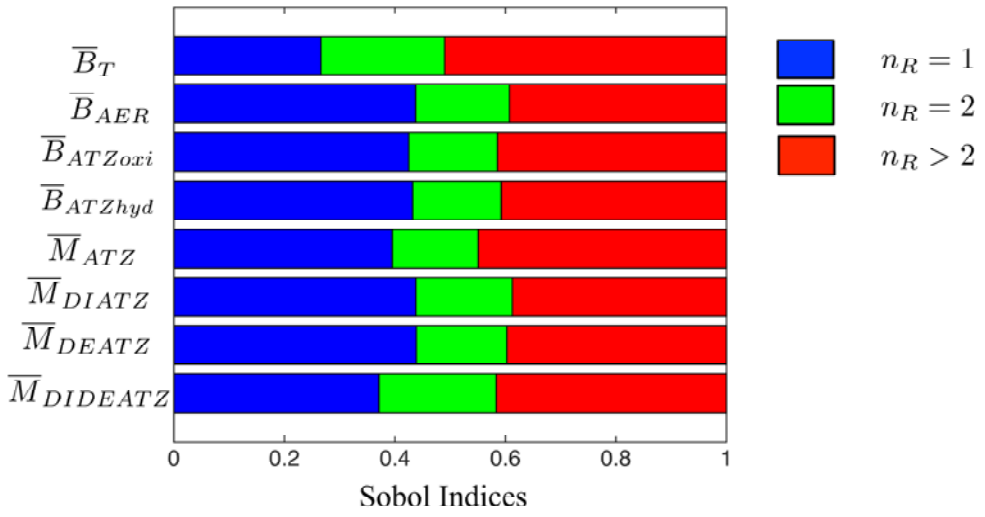

Figure 8: Analysis of variance: sum of principal indices $S^{(i,j)}$ associated with a single reaction ($n_R = 1$, blue bars), sum of indices accounting for joint variations of specific biomass affinities $\Phi_{i,j}$ associated with two ($n_R = 2$, green bars) or more ($n_R > 2$, red bars) reactions.

$\overline{B}_{\mathrm{ATZhyd}}$ for small values of $\Phi_{4,3}$ and large values of $\Phi_{4,1}$, where a conditional average of approximately 3×10^1 mg/m^2 is attained. Note that $\overline{B}_{\mathrm{ATZoxi}}$ (Figure 9b) displays a trend opposite to that of $\overline{B}_{\mathrm{ATZhyd}}$, i.e., microbial group $\mathrm{B_{ATZoxi}}$ thrives when $\Phi_{4,3}$ is large and $\Phi_{4,1}$ is small, while it tends to disappear for large $\Phi_{4,1}$ and small $\Phi_{4,3}$. A common feature observed in Figure 9a-b is that the average biomass of $\mathrm{B_{ATZoxi}}$ and $\mathrm{B_{ATZhyd}}$ attains values below 10^{-1} mg/m^2 when both $\Phi_{4,1}$ and $\Phi_{4,3}$ are smaller than 10^{-6} s^{-1}. These conditions favor the growth of $\mathrm{B_{AER}}$, as shown in Figure 9c.

Conditional averages of ATZ ($\mathrm{E}[\overline{M}_{\mathrm{ATZ}}|\Phi_{4,1}, \Phi_{4,3}]$ display relatively modest deviations around 10^{-3} mol/m^2. The microbial functional group $\mathrm{B_{ATZoxi}}$ is slightly more effective than $\mathrm{B_{ATZhyd}}$ in degrading ATZ (Figure 9a-b), as the smallest values for the conditional average of $\overline{M}_{\mathrm{ATZ}}$ are found for small $\Phi_{4,1}$

and large $\Phi_{4,3}$ values, where B_{ATZhyd} is scarce and B_{ATZoxi} thrives. Large values of $\overline{M}_{DIATZ}$ are found when B_{ATZoxi} prevails and ATZ is preferentially biodegraded by oxidative processes (Figure 9a-b). This is consistent with the reaction network structure, in that B_{ATZoxi} can degrade ATZ to DIATZ, which is then degraded by B_{ATZhyd}. The outputs $\overline{M}_{DEATZ}$ and $\overline{M}_{DIDEATZ}$ display a trend that is very similar to $\overline{M}_{DIATZ}$ and are therefore not shown here.

The combination of $\Phi_{4,1}$ and $\Phi_{4,3}$ also greatly affect the variability of the predicted biomass, quantified in terms of variance. The conditional variance associated with $\overline{B}_{ATZhyd}$ and $\overline{B}_{ATZoxi}$ is markedly reduced when $\Phi_{4,1} \gg \Phi_{4,3}$ and $\Phi_{4,1} \ll \Phi_{4,3}$, i.e., away from the bisector of the parameter space considered (Figure 9d-e), while $\mathrm{Var}[\overline{B}_{ATZhyd}|\Phi_{4,1}, \Phi_{4,3}] \approx \mathrm{Var}[\overline{B}_{ATZhyd}]$ along the bisector. This means that the variance (or uncertainty) associated with the biomass is not reduced when $\Phi_{4,1} \approx \Phi_{4,3}$, that is, the biomass growth is not governed by consumption of CH_2O when $\Phi_{4,1} \approx \Phi_{4,3}$, but is associated with biodegradation of ATZ or metabolites. A similar behavior can be observed for $\overline{B}_{ATZoxi}$.

Results in Figure 9 suggest that the ratio between values of $\Phi_{i,j}$ indicates which functional groups is favoured between two (or more) competing for the same substrate. We now conclude our analysis by quantifying the impact of the dimensionless ratios $\theta^{4,1}_{4,2} = \Phi_{4,1}/\Phi_{4,2}$, $\theta^{4,1}_{4,3} = \Phi_{4,1}/\Phi_{4,3}$, $\theta^{4,3}_{4,2} = \Phi_{4,3}/\Phi_{4,2}$ on biomass growth. Figure 10a-c depicts the sample probability (or relative frequency), denoted as P, of $\overline{B}_{ATZhyd}$ conditional to values of $\theta^{4,1}_{4,3}$ and $\theta^{4,1}_{4,2}$, which define the ratio of specific biomass affinity linked to biodegradation of CH_2O by B_{ATZhyd} with respect to B_{ATZoxi} and B_{AER}. We separate model realizations across diverse subpanels according to the values of $\theta^{4,1}_{4,3}$, with the corresponding class of values of $\theta^{4,1}_{4,2}$ identified by colored bars. Here, we identify conditional distributions by selecting realizations where $\theta^{4,1}_{4,3} > 2$ and $\theta^{4,1}_{4,3} < 0.5$. For simplicity, we label as $\theta^{4,1}_{4,3} \approx 1$ all realizations for which $0.5 \leq \theta^{4,1}_{4,3} \leq 2$. Similar notations are employed for $\theta^{4,1}_{4,2}$ and $\theta^{4,3}_{4,2}$.

The use of the dimensionless ratios allows identifying regimes of biomass growth across the uncertain parameters domain. The biomass present at long-term steady-state, as well as the mass of ATZ metabolites, displays important variations when considering diverse kinetics of CH_2O metabolism for each of the functional groups (figures 9 and 10), a situation that has been ignored in previus modeling efforts. In particular, when B_{ATZhyd} is faster than competitors in consuming CH_2O (i.e., $\theta^{4,1}_{4,3} > 2$ and $\theta^{4,1}_{4,2} > 2$), $\overline{B}_{ATZhyd}$ ranges from 10 to 100 mg/m^2 (blue bars in Figure 10a). Conversely, when $\theta^{4,1}_{4,3} < 0.5$ (i.e., $\Phi_{4,3}$ is larger than $2\Phi_{4,1}$) and $\theta^{4,3}_{4,2} > 2$, large concentrations of B_{ATZoxi} arise (blue bars in Figure 10f). The B_{ATZoxi} biomass typically tends to vanish when B_{ATZoxi} is the slowest group in consuming CH_2O ($\theta^{4,1}_{4,3} > 2$ and $\theta^{4,3}_{4,2} < 0.5$, red bars in Figure 10d). Under these conditions a few realizations predict $\overline{B}_{ATZoxi} \approx 10^0$ mg/m^2. Our results suggest that CH_2O is mostly consumed by B_{ATZhyd} and B_{AER} in these particular occurrences, and that B_{ATZoxi} growth is associated only with biodegradation of ATZ (and metabolites).

4. Conclusions

This work analyzes propagation of uncertainty within the reaction network of atrazine biodegradation in soils. Our purpose is to characterize long term impacts of ATZ application in soils through a probabilistic approach, where biokinetic parameters are assumed as stochastic inputs, as well as to rank the importance of the bioreactive processes included in the network.

Our work leads to the following major conclusions:

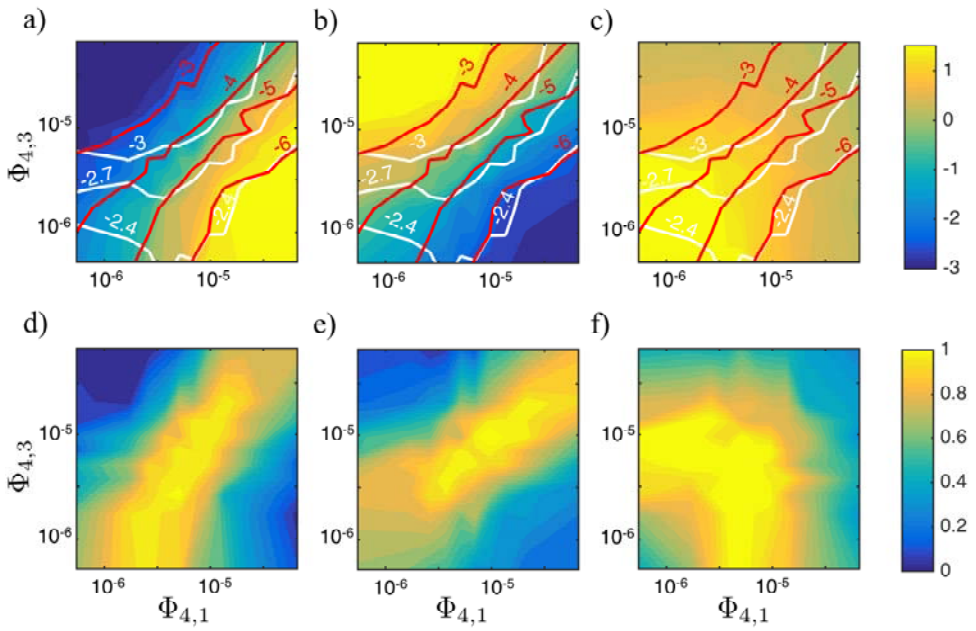

Figure 9: Contour map of (a-c) $\mathrm{E}[\log_{10}\overline{B}_s|\Phi_{4,1},\Phi_{4,3}]$ and (d-f) normalized conditional variance $\mathrm{Var}[\log_{10}\overline{B}_s|\Phi_{4,1},\Phi_{4,3}]/\mathrm{Var}[\log_{10}\overline{B}_s]$, where s stands for (a,d) ATZhyd, (b,e) ATZoxi, (c,f) AER. In (a-c) white contour lines and labels represent $\mathrm{E}[\log_{10}\overline{M}_{\mathrm{ATZ}}|\Phi_{4,1},\Phi_{4,3}]$ and red contour lines and labels represent $\mathrm{E}[\log_{10}\overline{M}_{\mathrm{DIATZ}}|\Phi_{4,1},\Phi_{4,3}]$

1. The key model outputs display sample pdfs which are bi- or multimodal. This can be seen as a result of the nonlinearity of the system. The biomass of different microbial functional groups also displays a multimodal pdf, which can be related to the ability of each microbial group to consume diverse substrates. The total biomass found in the soil column displays a range of variability limited to one order of magnitude, and its sample pdf displays a unimodal shape. Hence the total biomass in the soil column is chiefly governed by bacterial growth on organic matter (i.e., CH_2O) metabolism rather than on ATZ biodegradation. Our analysis suggests that multimodality emerges when competing bioreactive processes are modeled in a substrate-limited regime. This situation is common in agroecosystems, as well as other biogeochemical settings. Future developments for the analysis of uncertainty propagation in this type of systems are foreseen.
2. Coupling between processes has a relevant influence on the long-term soil biogeochemistry. Variations of a single kinetic parameter typically display limited impact on the mean and variance of the outputs. The combined variability in the kinetics of two or more biogeochemical processes largely contributes to the output uncertainty, as quantified in terms of variance by means of Sobol' indices. The moment-based sensitivity indices ($AMAE$ and $AMAV$) can provide a more comprehensive understanding of the complex reactive network because they target multiple moments of the pdfs of the quantities of interest. The $AMAV$ indices can capture links within complex reaction networks that are otherwise shadowed when using only the Sobol' indices. We foresee this behaviour may be shared by other biogeochemical systems, and in particular when biodegradation of agrochemicals is considered.
3. The specific biomass affinity is a valuable quantity to estimate biomass growth when multiple microbial functional groups compete for a substrate. We show that the ratio between the specific biomass affinities associated with two different functional group allows identifying regions of the

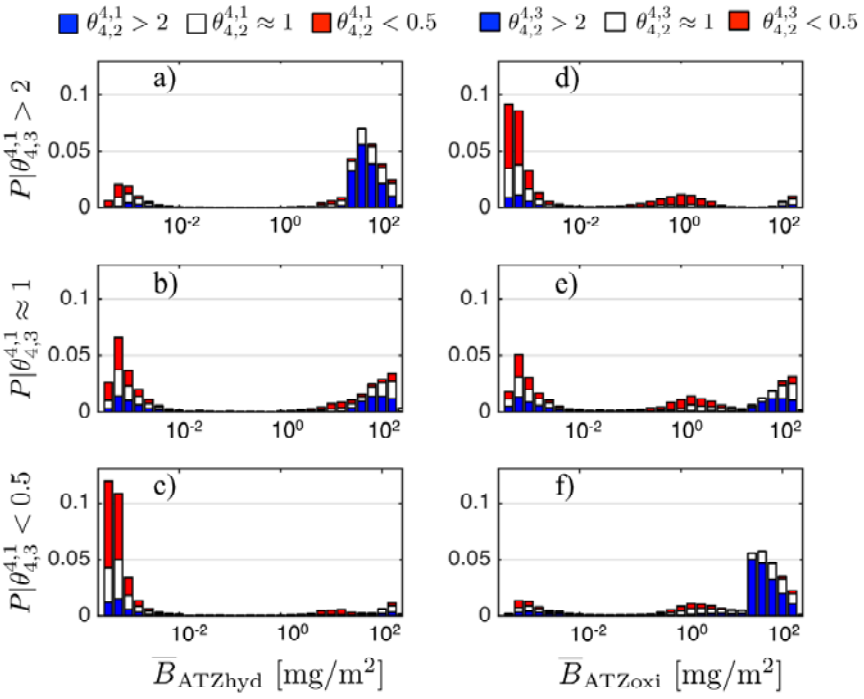

Figure 10: Sample probabilities of $\overline{B}_{\mathrm{ATZhyd}}$ (a-c) and $\overline{B}_{\mathrm{ATZoxi}}$ (d-f) conditional to values of $\theta^{4,1}_{4,3}$, $\theta^{4,1}_{4,2}$, $\theta^{4,3}_{4,2}$.

parameter space where a microbial group prevails. These regions are strictly linked to the pattern of the peaks observed in the output sample pdfs. This result is conducive to the characterization of the long-term ecological equilibrium in soils, i.e. to the identification of regimes where oxidative or hydrolytic microbial functional groups prevail.

4. We start our analysis from the set of model parameter values estimated by [34, 35] against laboratory experiments published in the literature. These datasets typically consider one microbially-driven kinetic process at a time. Our results indicate that constraining predictions of ATZ fate would require experiments targeting the coupled dynamics between different kinetic processes, driven in turn by different microbial communities. In particular, it would be highly desirable to obtain data to constrain the uncertainty related to the kinetics of CH_2O metabolism by the different microbial communities, when such a metabolic process takes place jointly with ATZ biodegradation. This

uncertainty currently hampers a prior reliable estimation of the ATZ fate, and it is the primary cause of the multimodal statistical distribution of target outputs that emerges from our analysis. The suite of numerical techniques that we have illustrated may be used for the design of novel experiments aimed at analyzing biodegradation of ATZ, as well as other agrochemicals.

Acknowledgments The authors acknowledge the Sydney Informatics Hub and the University of Sydney's high performance computing cluster Artemis for providing the high performance computing resources that have contributed to the research results reported within this paper. G.M. Porta and A. Guadagnini would like to thank the EU and MIUR for funding, in the frame of the collaborative international Consortium (WE-NEED) financed under the ERA-NET WaterWorks2014 Cofunded Call. This ERA-NET is an integral part of the 2015 Joint Activities developed by the Water Challenges for a Changing World Joint Programme Initiative (Water JPI). F. Maggi and D. la Cecilia were supported by the Sydney Research Excellence Initiative (SREI2020) of the University of Sydney. F. Maggi was also supported by the 2018 Mid-Career Research Award and by the Civil Engineering Research and Development Scheme (CERDS2015) of the University of Sydney. The BRTSim solver package can be downloaded at

https://www.dropbox.com/sh/wrfspx9f1dvuspr/AAD5iA9PsteX3ygAJxQDxAy9a?dl=0

Appendix A. Detailed biogeochemical parameterization of ATZ biodegradation network

Pathway	Reaction label	Kinetic biological aqueous reaction	Kinetic Parameters		
			r {k} $\left(\frac{1}{s}\right)$	K (MM) {k} $\left(\frac{mol}{l}\right)$	K (I) $\left(\frac{mol}{l}\right)$
P1R1a[a]	$R_{1,1}$	$C_8H_{14}ClN_5$ (ATZ) + H_2O(aq) → $C_8H_{15}N_5O$ (HOATZ) + H^+ + Cl^-	3.67×10^{-5} {1}	(I) 3.89×10^{-4} {3}	
P1R1b[b]	$R_{1,2}$	$C_8H_{14}ClN_5$ (ATZ) + H_2O(aq) → $C_8H_{15}N_5O$ (HOATZ) + H^+ + Cl^-	2.31×10^{-6} {4}	(I) 3.43×10^{-6} {6}	1.59×10
P1R1b[b]	$R_{6,1}$	CH_2O(aq) + $2\,NO_3^-$ → $2\,NO_2^-$ + CO_2 + H_2O	7.91×10^{-5} {67}	2.55×10^{-7} {69}	2.50×10
				4.70×10^{-3} {70}	2.50×10
P1R1b[b]	$R_{6,2}$	$2\,CH_2O$(aq) + $2\,NO_2^-$ → N_2(aq) + $2\,CO_2$ + $2\,H_2O$	9.23×10^{-6} {71}	8.87×10^{-7} {73}	2.50×10
				8.60×10^{-3} {74}	2.50×10
P1R2[c]	$R_{1,3}$	$C_8H_{15}N_5O$ (HOATZ) + H_2O(aq) → $C_6H_{10}N_4O_2$ (NIPA) + C_2H_7N (ETA)	3.77×10^{-5} {7}	(I) 3.14×10^{-5} {9}	
P1R3[d]	$R_{1,4}$	$C_6H_{10}N_4O_2$ (NIPA) + H_2O(aq) → $C_3H_3N_3O_3$ (CYA) + C_3H_9N (IPA)	3.89×10^{-4} {10}	(I) 7.80×10^{-4} {12}	
P2R1[e]	$R_{2,1}$	$C_8H_{14}ClN_5$ (ATZ) + $\frac{3}{2}\,O_2$(aq) → $C_5H_8ClN_5$ (DIATZ) + $3\,CH_2O$	1.61×10^{-4} {13}	(II) 2.25×10^{-3} {15}	
P2R2[f]	$R_{2,2}$	$C_5H_8ClN_5$ (DIATZ) + H_2O(aq) → $C_5H_9N_5O$ (DIHOATZ) + H^+ + Cl^-	1.23×10^{-5} {16}	(I) 1.98×10^{-4} {18}	
P2R3[g]	$R_{2,3}$	$C_5H_9N_5O$ (DIHOATZ) + H_2O(aq) → $C_5H_8N_4O_2$ (DHONATZ) + NH_3(aq)	1.23×10^{-5} {19}	(I) 1.98×10^{-4} {21}	
P2R4[g]	$R_{2,4}$	$C_5H_8N_4O_2$ (DIHONATZ) + H_2O(aq) → $C_3H_3N_3O_3$ (CYA) + C_2H_7N (ETA)	1.23×10^{-5} {22}	(I) 1.98×10^{-4} {24}	
P3R1[e]	$R_{3,1}$	$C_8H_{14}ClN_5$ (ATZ) + $3\,O_2$(aq) → $C_6H_{10}ClN_5$ (DEATZ) + $2\,H_2O$(aq) + $2\,CO_2$(aq)	1.51×10^{-4} {25}	(II) 2.09×10^{-3} {27}	
P3R2[f]	$R_{3,2}$	$C_6H_{10}ClN_5$ (DEATZ) + $\frac{3}{2}\,O_2$(aq) → $C_3H_4ClN_5$ (DIDEATZ) + $3\,CH_2O$	5.21×10^{-6} {28}	(II) 3.68×10^{-3} {30}	
P3R3[h]	$R_{3,3}$	$C_3H_4ClN_5$ (DIDEATZ) + H_2O(aq) → $C_3H_3ClN_4O$ (CLHOATZ) + NH_3(aq)	5.21×10^{-6} {31}	(I) 3.68×10^{-3} {33}	
P3R4[h]	$R_{3,4}$	$C_3H_3ClN_4O$ (CLHOATZ) + H_2O(aq) → $C_3H_4N_4O_2$ (DHOATZ) + H^+ + Cl^-	5.21×10^{-6} {34}	(I) 3.68×10^{-3} {36}	
P3R5[h]	$R_{3,5}$	$C_3H_4N_4O_2$ (DHOATZ) + H_2O(aq) → $C_3H_3N_3O_3$ (CYA) + NH_3(aq)	5.21×10^{-6} {37}	(I) 3.68×10^{-3} {38}	
P4R1[i]	$R_{5,1}$	$C_3H_3N_3O_3$ (CYA) + H_2O(aq) → $C_2H_5N_3O_2$ (BIU) + CO_2	2.14×10^{-3} {49}	(III) 6.70×10^{-1} {51}	
P4R2[i]	$R_{5,2}$	$C_2H_5N_3O_2$ (BIU) + H_2O(aq) → $C_2H_4N_2O_3$ (ALP) + NH_3(aq)	3.41×10^{-4} {52}	(III) 8.67×10^{-2} {54}	
P4R3[i]	$R_{5,3}$	$C_2H_4N_2O_3$ (ALP) + H_2O(aq) → $2\,NH_3$(aq) + $2\,CO_2$(aq)	9.26×10^{-5} {55}	(III) 1.11×10^{-1} {57}	
P5[l]	$R_{5,4}$	C_2H_7N (ETA) + $\frac{1}{2}O_2$(aq) → $2\,CH_2O$ + NH_3(aq)	9.34×10^{-5} {58}	(III) 8.38×10^{-1} {60}	
P6R1[m]	$R_{5,5}$	C_3H_9N (IPA) + H_2O(aq) → C_3H_8O (IPP) + NH_3(aq)	9.34×10^{-5} {61}	(III) 8.38×10^{-1} {63}	
P6R2[m]	$R_{5,6}$	C_3H_8O (IPP) + $\frac{3}{2}O_2$(aq) → $3\,CH_2O$ + H_2O(aq)	9.34×10^{-5} {64}	(III) 8.38×10^{-1} {66}	
R1[a]	$R_{4,1}$	CH_2O(aq) + O_2(aq) → H_2O(aq) + CO_2(aq)	5.60×10^{-5} {40}	0.75×10^{-3} {42}	
R2[n]	$R_{4,3}$	CH_2O + O_2(aq) → H_2O(aq) + CO_2(aq)	5.60×10^{-5} {46}	0.75×10^{-3} {48}	
R3[n]	$R_{4,2}$	CH_2O + O_2(aq) → H_2O(aq) + CO_2(aq)	5.60×10^{-5} {43}	0.75×10^{-3} {45}	
R4[o]		NH_3 + 3/2 O_2(aq) → H_2O(aq) + NO_2^- + H^+	1.0694×10^{-5}	3.0410×10^{-4}	
R5[o]		NO_2^- + 1/2 O_2(aq) → NO_3^-	3.5966×10^{-5}	(IV) 2.9840×10^{-4}	
R6[o]		NO_3^- + 1/2 CH_2O(aq) → 1/2 HCO_3^- + 1/2 H^+ + NO_2^-	4.0704×10^{-4}	2.0677×10^{-4}	2.50×10
		NO_3^- + 1/2 CH_2O(aq) → 1/2 HCO_3^- + 1/2 H^+ + NO_2^-	4.0704×10^{-4}	2.0703×10^{-4}	2.50×10
R7[o]		NO_2^- + 1/4 CH_2O(aq) + 3/4 H^+ → 1/4 HCO_3^- + NO(aq) + 1/2 H_2O	9.6768×10^{-5}	(IV) 7.4892×10^{-4}	2.50×10
		NO_2^- + 1/4 CH_2O(aq) + 3/4 H^+ → 1/4 HCO_3^- + NO(aq) + 1/2 H_2O	9.6768×10^{-5}	1.3599×10^{-4}	2.50×10
R8[o]		NO(aq) + 1/4 CH_2O(aq) → 1/4 H^+ + 1/4 HCO_3^- + 1/2 N_2O(aq)	8.0080×10^{-4}	1.7551×10^{-4}	2.50×10
		NO(aq) + 1/4 CH_2O(aq)* → 1/4 H^+ + 1/4 HCO_3^- + 1/2 N_2O(aq)	8.0080×10^{-4}	6.2404×10^{-5}	2.50×10
R9[o]		N_2O(aq) + 1/2 CH_2O(aq) → 1/2 H^+ + 1/2 HCO_3^- + 1 N_2(aq)	1.6846×10^{-5}	5.1698×10^{-5}	2.50×10
		N_2O(aq) + 1/2 CH_2O(aq) → 1/2 H^+ + 1/2 HCO_3^- + 1 N_2(aq)	1.6846×10^{-5}	8.8059×10^{-5}	2.50×10
		Kinetic chemical aqueous reaction	μ	K (MM)	
R10[o]		NO_2^- + 2/3 H^+ → 1/3 H_2O + 1/3 NO_3^- + 2/3 NO(aq)	1.0742×10^{-11}	1.129×10^{-4}	

R11$^{(p)}$	SOM $\rightarrow$ CH_2O + 0.039 NH_4^+	1.0×10^{-11} -
	Equilibrium aqueous complexation reactions (at T = 25°)	$\log_{10}(K_{(aq)})$
R12$^{(q)}$	$OH^- + H^+ \rightleftharpoons H_2O$(aq)	13.99
R13$^{(q)}$	$NH_4^+ \rightleftharpoons H^+ + NH_3$(aq)	-9.24
R14$^{(q)}$	CO_2(aq) + $H_2O \rightleftharpoons H^+ + HCO_3^-$	-6.34
	Equilibrium gas dissolution reactions (at 25°)	$\log_{10}(K_{(g)})$
R15$^{(q)}$	O_2(aq) $\rightleftharpoons$ O_2(g)	2.8980
R16$^{(q)}$	CO_2(g) + H_2O(aq) $\rightleftharpoons$ $H^+ + HCO_3^-$	-7.8136
R17$^{(q)}$	NH_3(g) + $H^+ \rightleftharpoons NH_4^+$	11.038
R18$^{(q)}$	N_2(aq) $\rightleftharpoons$ N_2(g)	3.2451
R19$^{(q)}$	NO(aq) $\rightleftharpoons$ NO(g)	2.7609
R20$^{(q)}$	N_2O(aq) $\rightleftharpoons$ N_2O(g)	1.6021
R21$^{(q)}$	Cl_2(g) + $H_2O \rightleftharpoons$ 1/2 O_2(aq) +2 Cl^- + 2 H^+	1.5516
	Equilibrium protection reactions (at 25°)	$\log_{10}(K_{(p)})$
R22$^{(r)}$	$NH_4^+ \rightleftharpoons NH_4^+$(p)	-0.336
R23$^{(s)}$	$NO_3^- \rightleftharpoons NO_3^-$(p)	-1.072
R24$^{(t)}$	$NO_2^- \rightleftharpoons NO_2^-$(p)	-1.072
R25$^{(u)}$	$Cl^- \rightleftharpoons Cl^-$(p)	-1.072
R26$^{(v)}$	ATZ $\rightleftharpoons$ ATZ(p)	0.515
R27$^{(z)}$	HOATZ $\rightleftharpoons$ HOATZ(p)	0.655
R28$^{(aa)}$	DIATZ $\rightleftharpoons$ DIATZ(p)	0.409
R29$^{(bb)}$	DEATZ $\rightleftharpoons$ DEATZ(p)	0.066
R30$^{(cc)}$	NIPA $\rightleftharpoons$ NIPA(p)	0.655
R31$^{(dd)}$	ETA $\rightleftharpoons$ ETA(p)	-0.9133
R32$^{(cc)}$	DIHOATZ $\rightleftharpoons$ DIHOATZ(p)	0.655
R33$^{(ee)}$	DIDEATZ $\rightleftharpoons$ DIDEATZ(p)	0.409
R34$^{(cc)}$	DIHONATZ $\rightleftharpoons$ DIHONATZ(p)	0.655
R35$^{(ee)}$	CLHOATZ $\rightleftharpoons$ CLHOATZ(p)	0.409
R36$^{(ff)}$	DHOATZ $\rightleftharpoons$ DHOATZ(p)	-1.18
R37$^{(gg)}$	CYA $\rightleftharpoons$ CYA(p)	0.0050
R38$^{(hh)}$	IPA $\rightleftharpoons$ IPA(p)	-0.9133
R39$^{(ii)}$	BIU $\rightleftharpoons$ BIU(p)	0.0050
R40$^{(ii)}$	ALP $\rightleftharpoons$ ALP(p)	0.0050
R41$^{(ll)}$	IPP $\rightleftharpoons$ IPP(p)	-1.5823

B_{ATZhyd} encompasses the genus *Bacillus*, *Pseudomonas*, and *Burkholderia*, and the strains *Pseudomonas* sp. ADP and *Nocardia* sp.; B_{ATZoxi} encompasses th strains TE1 and B30; B_{AER} encompasses the strain *Pseudomonas* sp. ADP, *Arthrobacter* P1, and *Mycobacteriumconvolutum* NPA-1, and an unidentified comm *Pseudomonas* and *Thiobacillum*; B_{AOB} encompasses the genus *Nitrosomona* and *Nitrosospira*; B_{NOB} encompasses the genus *Nitrobacter* and *Nitrospira*.

(a) Parameters estimated in [34] against experiments in [31, 41, 49, 55, 56]; (b) Parameters estimated in [34] against experiments in [31]; (c) Parameters estimated ag
experiments in [7]; (e) Parameters against experiments in [3, 2, 59]; (f) Parameters estimated against experiments in [2, 53, 59]; (g) Parameters assumed to be similar
those in P3R2; (i) Parameters estimated against experiments in [42]; (l) Parameters estimated against experiments in [36]; (m) Parameters assumed to be similar to th
R1; (o) Parameters estimated in [39] against experiments in [63]; (p) Parameters assumed in [39] after[17]; (q) Parameters from EQ3/6 [65]; (r) Parameters estimated i
in [61] against experiments in [37]; (t) Parameters assumed to be similar to those of NO_3^- as in [61]; (u) Parameters estimated in [61] against experiments in [1]; (v
Parameters estimated against experiments in [64]; (aa)Parameters estimated against experiments in [64]; (bb)Parameters estimated against experiments in [64]; (cc)
Parameters converted from [28]; (ee) Parameters assumed to be similar to those of DIATZ; (ff) Parameters assumed to be similar to those of Sarcosine, which were es
converted from [67]; (hh) Parameters assumed to be similar to those of ETA; (ii) Parameters assumed to be similar to those of CYA; (ll) Parameters converted from [
order of appearance of corresponding reactants. The Roman number in front of the MM constant refers to the list of MM terms used to account for substrate competit
list accordingly: (I) ATZ in P1R1a and P1R1b, HOATZ in P1R2, NIPA in P1R3, DIATZ in P2R2, DIHOATZ in P2R3, DIHONATZ in P2R4, DIDEATZ in P3R3, CL
P3R1, DEATZ in P3R2; (III) CYA in P4R1, BIU in P4R2, ALP in P4R3, ETA in P5, IPA in P6R1, IPP in P6R2; (IV) NO_2^- in R5 and R7. All kinetic biological aquec
relative to H^+ concentration with constants 10^{-8} and 10^{-6} M, respectively. Oxidative reactions also include a MM term relative to O_2(aq) concentration with const
R5. Anaerobic reactions also include an inhibition term relative to O_2(aq) concentration with constant 2.5×10^{-6} in P1R1b, and from R6 to R9. The microbial mortal
and B_{AER}, 2.69×10^{-6} s^{-1} for B_{AOB}, 1.61×10^{-6} s^{-1} for B_{NOB}, 1.22×10^{-7} s^{-1} for B_{DEN}.

Table A.1: Equilibrium and kinetic reactions implemented in the ATZ biochemical reaction network integrated with the nitrogen cycle and corresponding parameters. Number in {· } indicate the numbering k assigned to each uncertain parameter in the vector $\mathbf{p}$

Appendix B. Dimensionless form of transport equation

The specific biomass affinity is introduced in [34] to characterize the kinetic process expressed by Eqs.(1)-(2), as

$$\Phi = \frac{r}{Y K_{1_{MM}}} \tag{B.1}$$

The significance of Φ can be explained upon resorting to a dimensionless formulation of the one-dimensional transport equation for a substrate X in the presence of a single microbial functional group B and neglecting inhibition and competition terms appearing in (1). The latter can then be written as

$$\frac{\partial X'}{\partial t'} + \frac{\partial}{\partial z'}\left(X'u' - \frac{1}{Pe}\frac{\partial X'}{\partial z'}\right) = \frac{h}{U}\Phi\widetilde{B}\frac{X'}{X'+1}B' \tag{B.2}$$

where $z = hz'$, h is a length scale (e.g., the reaction zone characteristic depth), u' is a dimensionless velocity, $X' = S/K$ is dimensionless concentration, $Pe = Uh/D$ is the Péclet number, D is the molecular diffusion coefficient, $B' = B/\widetilde{B}$ is dimensionless biomass concentration. The quantity Φ in Eq. (10) expresses a characteristic reaction time per unit biomass. The product $\Phi\widetilde{B}$ has dimension [1/s] and defines a characteristic reaction time at given biomass concentration. As a consequence, setting $\widetilde{B} = 1$ mg/L enables recognizing that the dimensionless quantity $\Phi h/U$ defines a ratio between advective transport and reaction time scales, i.e. it corresponds to the Damköhler number.

References

[1] A. Back, S. Waring, Adsorption of nitrate, chloride and sulfate by some highly weathered soils from south-west Queensland, Aust. J. Soil Res. 17 (1979) 271–282.

[2] R. Behki, S. Khan, Degradation of Atrazine, Propazine, and Simazine by *Rhodococcus* Strain B-30, J. Agric. Food Chem. 42 (5) (1994) 1237–1241.

[3] R. Behki, E. Topp, W. Dick, P. Germon, Metabolism of the Herbicide Atrazine by *Rhodococcus* Strains, Appl. Environ. Microbiol. 59 (6) (1993) 1955–1959.

[4] B. Bekins, E. Warren, E. Godsy, A comparison of zero-order, first-order and Monod biotransformation models., Ground Water 36 (2) (1998) 261–268.

[5] L. W. Belser, Population ecology of nitrifying bacteria., Annu. Rev. Microbiol. 33 (1989) 309–333.

[6] E. Borgonovo, X. Lu, E. Plischke, O. Rakovec, M. Hill, Making the most out of a hydrological model data set: Sensitivity analyses to open the model black-box, Water Resour. Res. 53 (9) (2017) 7933–7950.

[7] K. L. Boundy-Mills, M. L. D. E. Souza, R. T. Mandelbaum, The atzB gene of *Pseudomonas* sp . strain ADP encodes the second enzyme of a novel atrazine degradation pathway, Appl. Environ. Microbiol. 63 (3) (1997) 916–923.

[8] D. K. Button, J. C. Garver, Continuous culture of *Torulopsis utilis*: a kinetic study of oxygen limited growth, J. Gen. Microbiol. 45 (1966) 195–204.

[9] F. Campolongo, J. Cariboni, A. Saltelli, An effective screening design for sensitivity analysis of large models, Environ. Modell. Softw. 22 (2007) 1509–1518.

[10] F. Campolongo, A. Saltelli, J. Cariboni, From screening to quantitative sensitivity analysis. a unified approach, Comput. Phys. Commun. 182 (2011) 978–988.

[11] S. A. Clay, W. C. Koskinen, Characterization of Alachlor and Atrazine Desorption from Soils, Weed Sci. 38 (1) (1990) 74–80.

[12] H. Dai, M. Ye, A. Walker, X. Chen, A new process sensitivity index to identify important system processes under process model and parametric uncertainty, Water Resources Research 53 (4) (2017) 3476–3490.

[13] P. de Anna, J. Jimenez-Martinez, H. Tabuteau, R. Turuban, T. Le Borgne, M. Derrien, Y. Meheust, Mixing and reaction kinetics in porous media: An experimental pore scale quantification, Envir. Sci. Tech. 48 (1) (2013) 508–516.

[14] A. Dell'Oca, M. Riva, A. Guadagnini, Moment-based metrics for global sensitivity analysis of hydrological systems, Hydrol. Earth Syst. Sci. 21 (2017) 6219–6234.

[15] D. Ding, D. A. Benson, D. Fernàndez-Garcia, C. V. Henri, D. W. Hyndman, M. S. Phanikumar, D. Bolster, Elimination of the reaction rate "scale effect": Application of the lagrangian reactive particle-tracking method to simulate mixing-limited, field-scale biodegradation at the schoolcraft (mi, usa) site, Water Resour. Res. (2017) doi:10.1002/2017WR021103.

[16] J. Ding, Q. Zhao, L. Wei, Y. Chen, X. Shu, Ammonium nitrogen removal from wastewater with a three-dimensional electrochemical oxidation system, Water Sci. Technol. 68 (3) (2010) 552–559.

[17] A. Don, E. Schulze, Controls on fluxes and export of dissolved organic carbon in grasslands with contrasting soil types, Biogeochemistry 91 (2) (2008) 117–131.

[18] A. Ebrahimi, D. Or, Mechanistic modeling of microbial interactions at pore to profile scale resolve methane emission dynamics from permafrost soil, J. Geophys. Res. Biogeosci. 122 (5) (2017) 1216–1238, 2016JG003674.

[19] Y. Edery, G. Porta, A. Guadagnini, H. Scher, B. Berkowitz, Characterization of bimolecular reactive characterization of bimolecular reactive transport in heterogeneous porous media, Transport Porous Med. 115 (2) (2016) 291–310.

[20] N. Fajraoui, F. Ramasomanana, A. Younes, T. Mara, P. Ackerer, A. Guadagnini, Use of global sensitivity analysis and polynomial chaos expansion for interpretation of non-reactive transport experiments in laboratory-scale porous media, Water Resour. Res. 47(2) (2011) W02521.

[21] W. Q. Fan, T. Yanase, H. Morinaga, S. Gondo, T. Okabe, M. Nomura, T. Komatsu, K. I. Morohashi, T. B. Hayes, R. Takayanagi, H. Nawata, Atrazine-induced aromatase expression is SF-1 dependent: Implications for endocrine disruption in wildlife and reproductive cancers in humans, Environ. Health Perspect. 115 (5) (2007) 720–727.

[22] FAO, IIASA, ISRIC, ISSCAS, JRC, Harmonized World Soil Database (version 1.2), FAO, Rome, Italy and IIASA, Laxenburg, Austria.

[23] L. Formaggia, A. Guadagnini, I. Imperiali, V. Lever, G. Porta, M. Riva, A. Scotti, L. Tamellini, Global sensitivity analysis through polynomial chaos expansion of a basin-scale geochemical compaction model, Computat. Geosci. 17(1) (2013) 25–42.

[24] A. Freixa, S. Rubol, A. Carles-Brangari, D. Fernández-Garcia, A. Butturini, X. Sanchez-Vila, A. M. Romaní, The effects of sediment depth and oxygen concentration on the use of organic matter: An experimental study using an infiltration sediment tank, Sci. Tot. Environ. 540 (2016) 20–31.

[25] E. Friebele, A. Shimoyama, C. Ponnamperuma, Adsorption of protein and non-protein amino acids on a clay mineral: a possible role of selection in chemical evolution, J Mol Evol. 16 (3) (1980) 269–278.

[26] J. Gerritse, F. Schut, J. Gotishal, Modelling of mixed chemostat cultures of an aerobic bacterium, *Comamonas testosteroni*, and an anaerobic bacterium, *Veillonella alcalescens*: comparison with experimental data, Appl. Environ. Microbiol. 58 (1992) 1466–1476.

[27] B. Halaburka, G. Lefevre, R. Luthy, Evaluation of mechanistic models for nitrate removal in woodchip bioreactors, Environ. Sci. Technol. 51 (9) (2017) 5156–5164.

[28] C. Hansch, A. Leo, D. Hoekman, Exploring QSAR: Hydrophobic, electronic, and steric constants, American Chemical Society, 1995.

[29] T. B. Hayes, A. Collins, M. Lee, M. Mendoza, N. Noriega, A. A. Stuart, A. Vonk, Hermaphroditic, demasculinized frogs after exposure to the herbicide atrazine at low ecologically relevant doses., Proc. Natl. Acad. Sci. U. S. A. (99) (2002) 5476–5480.

[30] B. Hileman, Book on hormone disrupters stirs row, Chem. Eng. News 74 (12) (1996) 7.

[31] I. Katz, M. Green, Y. Ruskol, C. G. Dosoretz, Characterization of atrazine degradation and nitrate reduction by *Pseudomonas* sp. strain ADP, Adv. Environ. Res. 4 (3) (2000) 211–218.

[32] J. S. Kindred, M. A. Celia, Contaminant transport and biodegradation: 2. Conceptual model and test simulations, Water Resour. Res. 25 (1989) 1149–1159.

[33] A. Kumar, N. Singh, Atrazine and its metabolites degradation in mineral salts medium and soil using an enrichment culture, Environ. Monit. Assess. 188 (3) (2016) 1–12.

[34] D. la Cecilia, F. Maggi, Kinetics of atrazine, deisopropylatrazine, and deethylatrazine soil biodecomposers, J. Environ. Manage. 183 (2016) 673–686.

[35] D. la Cecilia, F. Maggi, In-situ atrazine biodegradation dynamics in wheat (triticum) crops under variable hydrologic regime, J. Contam. Hydrol. 203 (2017) 104–121.

[36] P. R. Levering, L. Dijkhuizen, W. Harder, Metabolic regulation in the facultative methylotroph *Arthrobacter* P1. Growth on primary amines as carbon and energy sources, Arch. Microbiol. 139 (2) (1984) 188–195.

[37] Z. Li, R. Bowman, Retention of inorganic oxyanions by organo-kaolinite, Water Res 35 (16) (2001) 3771–3776.

[38] F. Maggi, BRTSim bio-reactive transport simulator v-2. A general-purpose multiphase and multicomponent computational solver for biogeochemical reaction-advection-dispersion processes in porous and non-porous media (2015).

[39] F. Maggi, C. Gu, W. J. Riley, G. M. Hornberger, R. T. Venterea, T. Xu, N. Spycher, C. Steefel, N. L. Miller, C. M. Oldenburg, A mechanistic treatment of the dominant soil nitrogen cycling processes: Model development, testing, and application, J. Geophys. Res. Biogeosci. 113 (G2) (2008) 1–13.

[40] F. Malaguerra, H.-J. Albrechtsen, P. J. Binning, Assessment of the contamination of drinking water supply wells by pesticides from surface water resources using a finite element reactive transport model and global sensitivity analysis techniques, J. Hydrol. 476 (Supplement C) (2013) 321 – 331.

[41] R. T. Mandelbaum, D. l. Allan, L. P. Wackett, Isolation and Characterization of a *Pseudomonas* sp. that Mineralizes the s-Triazine Herbicide Atrazine, Appl. Environ. Microbiol. 61 (4) (1995) 1451–1457.

[42] B. Martinez, J. Tomkins, L. P. Wackett, R. Wing, M. J. Sadowsky, Complete Nucleotide Sequence and Organization of the Atrazine Catabolic Plasmid pADP-1 from *Pseudomonas* sp. Strain ADP, J. Bacteriol. 183 (19) (2001) 5684–5697.

[43] W. Meylan, P. H. Howard, R. S. Boethling, Molecular topology/fragment contribution method for predicting soil sorption coefficients, Environ Sci Technol (26) (1992) 1560–1567.

[44] J. Monod, The Growth of Bacterial Cultures, Annu. Rev. Microbiol. 3 (1949) 371–394.

[45] M. Morris, Factorial sampling plans for preliminary computational experiments, Technometrics 33 (1991) 161–174.

[46] G. S. H. Pau, C. Shen, W. J. Riley, Y. Liu, Accurate and efficient prediction of fine-resolution hydrologic and carbon dynamic simulations from coarse-resolution models, Water Resour. Res. 52 (2) (2016) 791–812.

[47] A. Porporato, X. Feng, S. Manzoni, Y. Mau, A. J. Parolari, G. Vico, Ecohydrological modeling in agroecosystems: Examples and challenges, Water Resour. Res. 51 (7) (2015) 5081–5099.

[48] G. Porta, G. Ceriotti, J.-F. Thovert, Comparative assessment of continuum-scale models of bimolecular reactive transport in porous media under pre-asymptotic conditions, J. Contam. Hydrol. 185 (2016) 1–13.

[49] M. Radosevich, S. J. Traina, Y. L. Hao, O. H. Tuovinen, Degradation and mineralization of atrazine by a soil bacterial isolate, Appl. Environ. Microbiol. 61 (1) (1995) 297–302.

[50] S. Razavi, H. V. Gupta, What do we mean by sensitivity analysis? the need for comprehensive characterization of "global" sensitivity in earth and environmental systems models, Water Res. Resear. 51 (5) (2015) 3070–3092.

[51] W. J. Riley, F. Maggi, M. Kleber, M. S. Torn, J. Y. Tang, D. Dwivedi, N. Guerry, Long residence times of rapidly decomposable soil organic matter: application of a multi-phase, multicomponent, and vertically resolved model (BAMS1) to soil carbon dynamics, Geoscientific Model Development 7 (2014) 1335–1355.

[52] A. Saltelli, M. Ratto, T. Andres, F. Campolongo, J. Cariboni, D. Gatelli, M. Saisana, S. Tarantola, Global sensitivity analysis: the primer, John Wiley, 2008.

[53] Z. Q. Shao, W. Seffens, W. Mulbry, R. M. Behki, Cloning and expression of the s-triazine hydrolase gene (trzA) from *Rhodococcus corallinus* and development of recombinant strains capable of dealkylating and dechlorinating the herbicide atrazine, J. Bacteriol. 177 (20) (1995) 5748–5755.

[54] M. Shukla (ed.), Soil hydrology, land use and agriculture: measurement and modelling, 2003.

[55] D. Smith, S. Alvey, S. E. Crowley, Cooperative catabolic pathways within an atrazine-degrading enrichment culture isolated from soil, FEMS Microbiol. Ecol. 53 (2) (2005) 265–273.

[56] D. Smith, D. E. Crowley, Contribution of ethylamine degrading bacteria to atrazine degradation in soils, FEMS Microbiol. Ecol. 58 (2) (2006) 271–277.

[57] I. M. Sobol', Sensitivity estimates for nonlinear mathematical models, Math. Modeling Comput. Experiment 1 (4) (1993) 407–414 (1995).

[58] I. M. Sobol', On quasi-monte carlo integrations, Math. Comput. Simulat. 47 (2) (1998) 103 – 112.

[59] R. Solomon, A. Kumar, V. Satheeja Santhi, Atrazine biodegradation efficiency, metabolite detection, and trzD gene expression by enrichment bacterial cultures from agricultural soil., J. Zhejiang Univ. Sci. B 14 (12) (2013) 1162–1172.

[60] B. Sudret, Global sensitivity analysis using polynomial chaos expansions, Reliab. Eng. Syst. Safe. 93 (7) (2008) 964 – 979.

[61] F. H. M. Tang, F. Maggi, Breakdown, uptake and losses of human urine chemical compounds in barley (*Hordeum vulgare*) and soybean (*Glycine max*) agricultural plots. Effectiveness of human urine use in agriculture, Nutr. Cycl. Agroecosys. 104 (2) (2016) 221–245.

[62] M. T. Van Genuchten, A Closed-form Equation for Predicting the Hydraulic Conductivity of Unsaturated Soils, Soil Sci. Soc. Am. J. 44 (1980) 892–898.

[63] R. T. Venterea, D. E. Rolston, Nitric and nitrous oxide emissions following fertilizer application to agricultural soil: Biotic and abiotic mechanisms and kinetics, J. Geophys. Res. Atmos. 105 (D12) (2000) 15117–15129.

[64] Z. Vryzas, E. Papadopoulou-Mourkidou, G. Soulios, K. Prodromou, Kinetics and adsorption of metolachlor and atrazine and the conversion products (deethylatrazine, deisopropylatrazine, hydroxyatrazine) in the soil profile of a river basin, Eur. J. Soil Sci. 58 (5) (2007) 1186–1199.

[65] T. J. Wolery, EQ3/6, A Software Package for Geochemical Modeling of Aqueous Systems: Package Overview and Installation Guide (Version 7.0), lawrence Livermore National Laboratory, University of California, Livermore, California (1992).

[66] V. Yadav, G. Malanson, E. Bekele, C. Lant, Modeling watershed-scale sequestration of soil organic carbon for carbon credit programs, Applied Geography 29 (4) (2009) 488–500.

[67] S. Yalkowsky, Handbook of Aqueous Solubility Data, CRC Press, 2003.

[68] J. Zhao, T. Scheibe, R. Mahadevan, Model-based analysis of the role of biological, hydrological and geochemical factors affecting uranium bioremediation, Biotechnol. Bioeng. 108 (7) (2011) 1537–1548.